

Seismotectonics and 3-D Seismic Velocity Structure of the Arunachal Himalaya

P. Mahesh¹, G. Srijayanthi^{2,3}, M. Ravi Kumar^{2,*}

¹CSIR-National Institute of Oceanography, Goa -403004, India

²CSIR-National Geophysical Research Institute, Hyderabad - 500007, India

³Institute of Seismological Research, Gandhinagar, Gujarat, India

*Correspondingauthor:M. R. Kumar (mravingri@gmail.com)

Abstract

Knowledge of seimotectonics of Arunachal Himalaya holds the key to comprehend the complex deformation scenario in the eastern Himalayan syntaxial (EHS) zone comprising India, Eurasia and Burma plates. Data from a network of 41 broadband seismic stations operated from 2009 December to 2016 March in a hitherto unmonitored zone, enabled us to investigate the distribution of local seismicity and 3-D crustal velocity structure. Seismicity trends reveal that the western Arunachal and the EHS zone are seismically active compared to central Arunachal. Seismicity in western Arunachal extends to the south of Mikir Hills in the Foreland, where it is associated with a WNW-ESE trending dextral fault in the Indian crust. While the entire crust is seismically active in the syntaxial zone, earthquakes in central Arunachal are confined to the upper 20 km. Further, low V_P (~5.2-5.4 km/s) values in the sub-Himalaya indicate 5-6 km thick sediments. Low V_P/V_S (1.6-1.70) values in the mid-to-lower crustal depths may be associated with crustal anisotropy. Velocity images along with seismicity reveal a gently dipping Main Himalayan Thrust (MHT) without a clear signature of a mid crustal ramp in the region. The seismically less active flat portion of the MHT in central Arunachal region might be related to a partially creeping segment or less deformation at the Himalayan front.

Key Words: Arunachal Himalaya, Seismicity, Main Himalayan Thrust, Seismic tomography, 3-D velocity structure .

1 Introduction

The India-Eurasia collision in the Cenozoic led to a spectacular, convex orogeny, the ~2500 km long Himalayan mountain range (Rajendran et al., 2017). The continual accumulation of strain due to shallow angle thrusting of the Indian plate beneath the Eurasian plate at a convergence rate of 15-30 mm/yr (Jade et al., 2017) also resulted in many devastating large magnitude earthquakes along the Himalayan arc (Fig. 1a). Study of geodetic rates and earthquake distribution clearly indicates a non-uniform distribution and partitioning of strain, demarcating many seismic gaps along the Himalayan arc (Bilham & England, 2001; Avouac et al., 2015; Stevens and Avouac, 2016; Rajendran et al., 2017). A recent review also emphasized that several segments of the Himalaya are overdue for devastating earthquakes (Bilham, 2019). Previously, Hetenyi et al. (2016a) documented lateral variations along the Himalayan arc and segmented it into four distinct tectonic regions, namely the northwestern, Nepal, Bhutan and northeastern Himalaya, based on arc parallel gravity anomalies and topography.

The Arunachal region constitutes the easternmost part of Himalaya, between 26°N to 29°N and 91°E to 97°E. The region is subjected to complex stress accumulation owing to its proximity to the triple-junction of India, Eurasia and Burmese plates. Also, the region is bounded in the southwestern foreland by the Shillong plateau, Mikir hills and the Kopili fault (KF) (Fig.1b). These three intra-plate regions are seismically very active. The Mikir massif is believed to be a part of Shillong plateau that shifted northeast and presently separated by a ~400 km long and 100 km wide NW-SE trending KF, that probably extends into the Bhutan Himalaya. The KF is one of the most seismically active faults in the Assam valley (Nandy, 2001, Bhattacharya et al., 2008; Kayal et al., 2012). Results from GPS studies (Vernant et al., 2014, Barman et al., 2017) suggest that KF distinctly partitions the Assam valley into the Shillong and Assam blocks. A 2–3 mm/yr dextral slip occurs along this fault due to clockwise rotation of the Shillong block (Vernant et al., 2014; Barman et al., 2017.)

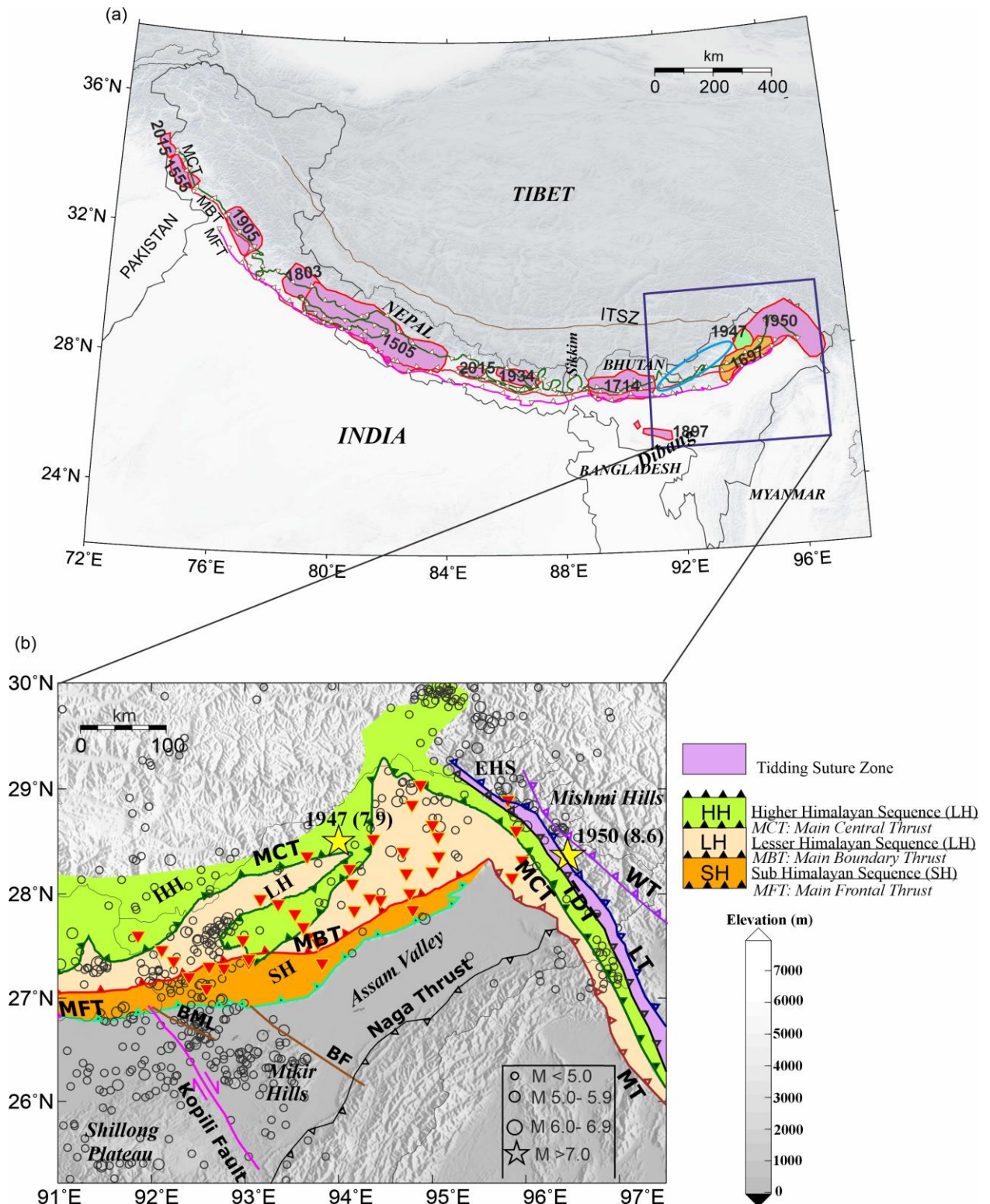


Figure 1. (a) Topographic map of the Himalayan arc showing rupture zones of large and great historical earthquakes from 18 century A.D. (after Pandey et al., 2021; Diehl et al., 2017; Bilham 2019), and the Arunachal seismic gap (blue ellipse). Blue rectangular box represents the study region (b) Seismicity map with major fault zones in the study region. Inverted triangles represent broadband seismicological stations whose data is utilized in the current study and open circles indicate moderate to major earthquakes ($M \geq 4.5$) from 1976 to 2021 (Source: USGS, 2017). Continuous lines trace the major thrusts viz., MFT: Main Frontal Thrust; MCT: Main Central Thrust; MBT: Main Boundary Thrust ; ITSZ: Indus-Tsangpo Suture Zone; TDT: Tidding thrust ; MT: Mishmi Thrust; LT: Lohith Thrust; WT: Walong Thrust. SH: Sub-Himalaya; LH: Lower Himalaya; HH: Higher Himalaya; EHS: Eastern Himalayan Syntaxis; BF: Bomdila Fault; BML: Bhairabkunda-Mazbat Lineament.

The Arunachal region experienced two large magnitude earthquakes, the M 8.6 1950 great Assam earthquake near the India, Eurasia and Burma plate junction and the M 7.7 1947 earthquake (Fig. 1b) in north central Arunachal (Chen & Molnar, 1977). This region is also located within the Assam seismic gap proposed by Khattri et al. (1983). A recent paleo seismic study along the Main Frontal Thrust (MFT) provided evidence for surface rupture of the 1697 Sadiya earthquake (Fig. 1a) in Arunachal, with its magnitude estimated in the range of M_w 7.7–8.1 (Pandey et al., 2021). Considering the fact that no great earthquakes occurred since 1697, a seismic gap has been postulated between the 1714 Bhutan and the 1947 Arunachal earthquakes, capable of hosting a M_w 8.4 earthquake (Hetényi, et al., 2016b; Bilham, 2019). Bilham (2019) also stated that the region between the 1947 Arunachal and the 1950 Assam earthquakes has the potential to slip and produce an earthquake of $M_w \geq 7.7$ akin to the 2015 Gorkha earthquake in Nepal.

The subduction of the Indian plate beneath Tibet is accommodated by the Main Himalayan Thrust (MHT), which is a source of megathrust earthquakes in the Himalaya (Seeber and Armbruster, 1981). Seismic images and seismicity distribution enabled detection of the MHT, mid-crustal ramp and constraining their geometry (Ni and Barazangi, 1984; Pandey et al., 1995; Schulte-Pelkum et al., 2005; Nábělek et al., 2009; Singer et al., 2017a). Since seismic hazard due to large magnitude Himalayan earthquakes mainly depends on the geometry of the MHT (Gupta et al., 2022; Dal Zilio et al., 2019), it is essential to decipher its variation along different segments of the Himalayan arc.

Numerous studies to comprehend the seismotectonics and crustal structure are conducted in the Himalayan region using data from temporary and permanent seismological networks. The focal depths of earthquakes in the Nepal Himalaya indicate a bimodal seismicity distribution, attributed to brittle deformation of the continental upper crust and upper mantle (Monsalve et al., 2006). Dal Zilio et al. (2019) attributed this bimodal seismicity to strong friction and complex non-planar geometry of the MHT. In contrast, results from northwestern (Mahesh et al., 2013), Sikkim (Hazarika et al., 2010) and Bhutan Himalaya (Diehl et al., 2017) reveal that the entire crust is seismogenic. Further, dominance of strike-slip earthquakes in Sikkim and Bhutan Himalayas indicates the active role of transverse tectonics (Hazarika et al., 2010, Diehl et al., 2017). Seismicity, moment tensor and local earthquake tomography studies corroborated a thick crust in western Bhutan, with dominance of transverse tectonics and a flat, silently creeping MHT in eastern Bhutan (Diehl et al., 2017). They also suggested that the transverse Dhubri-Chungthang fault (DCF), a potential feature that marks the western boundary of the Shillong block might cut across the MHT between Nepal and Bhutan. Results of ambient noise tomography from Bhutan show high shear wave velocity anomalies associated with

the local geometry of MHT indicating localized quartzite dominated rocks with duplex structures (Singer, et al., 2017b).

Compared to other parts of the Himalaya, very few seismological studies were conducted in the Arunachal region, mostly using data from a few stations. Kayal et al. (1993) studied the nature of seismicity in the vicinity of the Main Boundary Thrust (MBT) in Arunachal, using sparse networks of temporary stations operated during April-June 1986 and March-December 1990. They reported subcrustal earthquakes to the south of MBT down to a depth of 80 km and indication of transverse tectonics based on composite focal mechanisms that show strike-slip faulting. Kundu et al. (2020) studied variations in crustal thickness and composition using broadband data from a network of 11 seismic stations operated in the Lohit Valley in the Eastern Syntaxis during January 2007 and June 2008. This study reported earthquakes down to a depth of 35 km and a variation in crustal thickness from ~46 km beneath the Brahmaputra valley to ~55 km in the Lohit Plutonic Complex. Yadav et al. (2021) studied the seismicity pattern in Siang valley in the EHS using local earthquake data from a network of 8 broadband seismic stations and reported earthquakes down to a depth of 40 km. Shear velocity structure of northeast India, including Arunachal Himalaya and EHS, derived using data from 20 broadband seismic stations operated by the India Meteorological Department (IMD, India) during 2011-2013, revealed significant variation in crustal thickness within the EHS, suggesting complex crustal deformation (Kumar et al., 2021). Receiver function (RF) images of the crust beneath the Arunachal Himalaya constructed using data from 32 broadband seismic stations operated during 2010-2016, brought out a less complex crust and a mechanically weak middle crust, without prominent signatures of a mid-crustal ramp (Singh et al., 2021). Recently, Shukla et al. (2022) derived crustal thickness and Poisson's ratio in the northeastern Indian region using RF analysis of data from 19 broadband seismic stations operated by National Center for Seismology (NCS, India). This study correlated the high Poisson's ratio values in the Tiding suture zone of EHS with partially serpentinized rocks in the ophiolitic mélangé complex.

The Arunachal region is hitherto less investigated and the following important questions remain relevant: i) what is the correlation of local seismicity distribution with the major Himalayan thrust faults? ii) do earthquakes in this region follow a bimodal depth distribution implying brittle strength in the crust and upper mantle, or, is the whole crust seismogenic? iii) does the KF extend beneath the Himalaya? iv) is the tectonics of the Arunachal Himalaya distinct compared to the other segments of the Himalayan arc? With an aim to address the above issues, we present maiden results of local seismicity and 3D V_P (P - wave velocity) and V_P/V_S images of the Arunachal Himalaya using

arrival time data of P and S waves recorded by a local seismic network of 41 broadband stations (Fig.1b) operated from 2009 to 2016.

2. Geology and Tectonics of the Arunachal Himalaya

The most prominent tectonic features in Arunachal are the Main Central Thrust (MCT), Main Boundary Thrust (MBT) and the Main Frontal Thrust (MFT) (Fig.1b). The MCT represents the boundary between the Lower Himalayan (LH) sequence in the south and the Higher Himalayan (HH) crystalline rocks in the north. The MBT separates the sub-Himalaya (SH) and the Lower Himalaya. Interestingly, both the MBT and MFT are nearly parallel in the Arunachal Himalaya and the trend of MCT is undulating (Yin et al., 2010). The region is bounded by the Shillong Plateau to the southwest which is dominated by thrust faulting (Chen & Molnar, 1990) and pop-up tectonics (Rao and Kumar, 1997, Bilham & England, 2001), followed by a NW-SE trending transverse KF and Bomdila Fault (BF). Rakshit and Rakshit (2022) reported a WNW-ESE trending Bhairabkunda-Mazbat Lineament (BML) in the KF zone, that is transverse to KF. To the east, the Eastern Himalayan syntaxis (EHS) (Fig. 1b) marks a change in the tectonic regime from collision along the Himalaya to strike-slip faulting in south-eastern Tibet (Holt et al., 1991). The NW-SE trending Mishmi thrust (MT), Tidding thrust (TDT), Lohith thrust (LT) and the Walong thrust (WT) are the other major faults in this region, that are in proximity to the source zone of the 1950 M 8.6 earthquake. The Tidding suture in the Mishmi region is an extension of the Indus-Tsangpo Suture Zone (ITSZ) and marks the region where the MBT takes a sharp bend southwards and connects to the Indo-Burma Ranges. The NE-SW trending Naga Thrust to the south terminates near the NW-SE trending Mishmi Thrust which merges further with the Sagaing fault to the east of the Burma micro-plate (Pandey et al., 2017).

The Arunachal Himalaya is a region of great geological significance within a broader Himalayan mountain range. The lithological assembly of the region, characterized by complex tectonic processes, constitutes the Tethyan Sedimentary Sequence, Higher Himalayan Sequence, Lower Himalayan Sequence and the Siwalik Group, that have a bearing on the geological evolution of the area (Gansser 1964; Yin et al., 2010; Webb et al., 2013; DeCelles et al., 2016). Sedimentary rocks deposited in this marine environment during the Mesozoic and early Cenozoic era form the Tethyan Sedimentary Sequence consisting of shale, sandstone, limestone, and flysch deposits, indicating a once-vast oceanic basin (Gansser, 1964). The Higher Himalayan Sequence represents the crystalline core of the Himalayas and is composed of high-grade metamorphic rocks, including kyanite-sillimanite-bearing gneiss/ schist, migmatite, leucogranite, and amphibolites (Gururajan & Choudhary 2003; Yin et al., 2010; Webb et al., 2013; DeCelles et al., 2016). The Lower Himalaya, between the MBT and the MCT, is tectonically complex. The rocks in this region are a mix of Lower Himalayan

Sedimentary Sequences (LHSS) and Lower Himalayan Crystallines (LHC). LHSS consists of sandstone, shale, and limestone, that were deposited on the northern margin of the Indian plate prior to its collision with Eurasia. The LHC is composed of quartzites, phyllites, schists, and granitoids. The sub-Himalaya contains Siwalik group rocks, a prominent unit in Arunachal Himalaya, composed primarily of clastic sedimentary rocks like sandstone, siltstone, and conglomerate, deposited during the late Cenozoic in the foreland basin that formed due to the uplift of Himalayas. The Siwalik group preserves a record of tectonic and climatic changes in the region during the Himalayan uplift (Gansser, 1964; Kumar 2016). This group in Arunachal forms a ~5–6 km thick upward coarsening succession of fluvial and alluvial fan deposits (Decells 2016). The syntaxis is generally geologically referred to as a tectonic intersection point where many faults converge. In the study region, the Eastern Himalayan syntaxis is where all the three major tectonic units; the Sub-Himalaya (Siwaliks), Lesser Himalaya (including the Gondwana Group) and Higher Himalaya (Gansser, 1964) converge. These units are mainly situated on the western side (limb) of the syntaxis. On the eastern limb, two major units namely the Tidding Suture Zone and the Lohit Plutonic Complex are found, accompanied by a sequence of Eocene-age sedimentary rocks intermingled with basic volcanic rocks (Singh, 1993). The Tidding Suture Zone overriding the Mishmi crystalline, equivalent of the Higher Himalayan Crystalline on the southwest and bounded by the Lohit thrust on the northeast, contains rich preserves of ophiolitic mélange of mainly garnetiferous metavolcanics, marble bands, serpentinite, and graphitic-garnet schist (Gururajan & Choudhary 2003). The Lohit Plutonic Complex is further subdivided into the western and eastern belts separated by the Walong thrust (Gururajan & Choudhary 2003).

The Mikir Hills surrounded by Tertiary rocks with faulted contacts, located southwest of the Arunachal Himalaya, represent the final exposures of shield rocks and share similarities with the Shillong plateau. Drilling investigations in the northeast part of Mikir Hills indicate a highly faulted basement with approximately 3800 m of Tertiary and Quaternary sedimentary deposits (Mathur and Kohli, 1963).

3 Seismological Network and single event earthquake locations

The CSIR-National Geophysical Research Institute (NGRI), Hyderabad, India has operated a seismological network comprising 41 stations, from December 2009 to March 2017 (Fig. 1b), spanning 91.5°E to 96°E and 27°N to 29.5°N, from Tawang in the West to lower Dibang valley in the East. Owing to the rugged topography and poor road conditions, installation of such a dense network in an area like Arunachal has been a very challenging task. For the present study, data from December 2009 to March 2016 is utilized. The stations are a combination of REFTEK-151 seismometers with REFTEK 130 data acquisition systems (DAS), Trillium 120P seismometers with Taurus data loggers

and CMG-3T seismometers connected to REFTEK 130 data acquisition systems. The ground motion is recorded at 50 samples per second. The stations were installed in phases and the details are given in supplementary information (Table S1).

The first arrival times of P- and S-phases were picked manually, using the earthquake analysis software SEISAN (Havskov & Ottemöller, 2003). The average initial picking accuracy for the P-arrivals is 0.15 s and S- arrivals is 0.3 s. The local magnitude (M_L) is computed from the amplitudes of the horizontal components of seismograms. Initially, the hypocentral locations of individual events having at least 5 P- and 3 S- arrivals, were obtained using the HYPOCENTER program (Lienert & Havskov, 1995). Since no published velocity model exists for the study region, we tested 5 different models proposed for the NE Himalaya and nearby Nepal Himalaya. These are Gupta (1984) model (model-1), the P-wave velocity model (model-2) of De & Kayal, (1990), the local earthquake tomography model (model-3) of Bhattacharya, et al. (2010), the improved 1D velocity model for Nepal Himalaya (model-4) by McNamara et al. (2017) and the 1D velocity model (model-5) for Bhutan Himalaya derived by inversion of local earthquake data (Singer et al., 2017a). An average V_p/V_s value of 1.72 is used for estimation of initial hypocenter location parameters. The errors in the estimated hypocentral parameters using each of the above velocity models are shown in supplementary information (Fig. S1). It is found that the lateral distribution of earthquakes remains similar irrespective of the velocity models used for location. However, noticeable changes are observed in hypocentral depths, which tend to change from shallow to deep or vice-versa with change in the velocity models. The root mean square (RMS) errors corresponding to all the five models are mostly <1 s (Fig. S1). However, the largest value of the RMS error reaches 2 s, when the earthquake location parameters are estimated using model-1 and model-2. The least RMS is observed for velocity model-3 proposed by Bhattacharya, et al. (2010). A thorough analysis clearly reveals that this a priori model not only reduces the RMS value, but also improves the location errors to ≤ 5 km in latitude. Therefore, model-3 is used as the initial velocity model for preliminary location of earthquakes. A total of 1420 (Fig. S2) earthquakes in the magnitude range of M_L 1.0 to 5.2 are located in Arunachal and nearby regions. The frequency-magnitude distribution of seismicity indicates an M_C of 2.2 (Fig. S3). Many recorded events fall outside the network. It is well established that the precision of earthquake locations depends on the distribution of the recording stations, accurate phase arrival times and use of an appropriate velocity model between the sources and stations, especially in areas with large lateral heterogeneities (Okada et al., 1970). Therefore, apart from a minimum of 8 phase arrivals, we considered only those events for further analysis that have at least one nearest recording station within 150 km epicentral distance.

4 Minimum 1D velocity model

A subset of 121 (Fig. S4) earthquakes having an azimuthal gap $\leq 180^\circ$ and recorded by at least 6 stations (minimum 10 phases marked; 6 P and 4 S picks) is considered to determine a reliable velocity model using the VELEST program (Kissling, 1988; 1995). The simultaneous inversion scheme is used to invert for both the hypocenters and 1D velocity model with station corrections, using the five different velocity models mentioned above, as initial models (Fig. 2a). However, since the inversion results from model-3 produced the least RMS, we used this model as the initial one to compute the final minimum 1D velocity model. We divided this model into 2 km thick layers and also varied the V_p/V_s value from 1.72 to 1.74 to invert for both V_p and V_s simultaneously. In every iteration, layers having similar velocities were merged as a single layer and the inversion is repeated until the least RMS is obtained for all the earthquakes. The models (Fig. 2b) obtained from inversion are seen to resolve layers only to a depth of 40 km, owing to lack of head waves and hypocenters within deeper layers. The ray path and depth distribution of earthquakes are shown in Figures 2c,d. The final model (model 6) also reduces the average RMS error from 0.3 s to 0.2 s (Fig. S1).

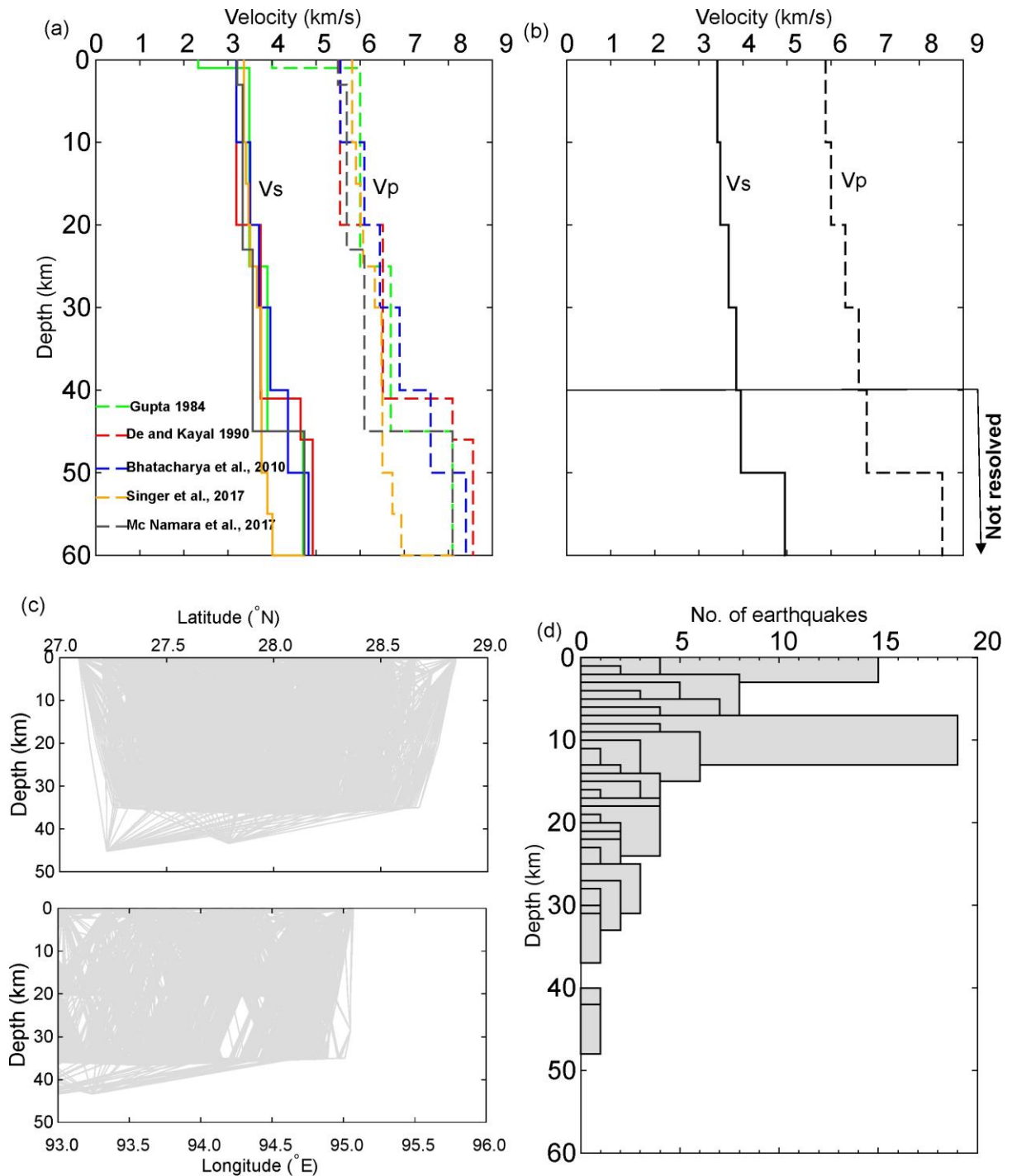


Figure 2. (a) Initial , (b) final velocity models, (c) ray path distribution in depth along latitude and longitude and (d) depth distribution of earthquakes relocated with the new minimum 1D model.

5 Relocated earthquakes and distribution of seismicity

The new 1D velocity model was then used to relocate 1418 earthquakes that are initially located (Fig. S2) using the HYPOCENTER program inbuilt in SEISAN (Havskov & Ottemöller, 2003). The earthquakes relocated using the velocity model obtained by VELEST along with their errors in latitude, longitude, depth and RMS time residuals are shown in Figure 3. The local magnitudes (M_L) of these earthquakes vary from 1.0 to 5.2. Two moderate magnitude earthquakes ($M_L \geq 5.0$) are recorded during

the study period. The earthquake locations were further constrained by relocating them with the double difference algorithm hypoDD (Waldhauser & Ellsworth, 2000). The double-difference (DD) technique utilizes the differential travel time data to solve for hypocentral locations and origin times of events. The advantage of this method is that it improves the relative location accuracy by minimizing errors arising from the unmodelled velocity structure. While relocating the earthquakes, it is ensured that the maximum epicentral distance is 200 km, the separation between a pair of events is less than 20 km and the number of neighbours per event does not exceed 8. For relocation, we used both the P and S phase data from the local earthquake catalog. A total of 759 clustered events are considered for relocation after discarding a few isolated ones that are not sufficiently linked with their neighbors. The DD relocated earthquakes are shown in Figure 4. The reliability of the relocated earthquakes is assessed using bootstrap analysis (Waldhauser & Ellsworth, 2000). The details are given in supplementary text and Figure S5.

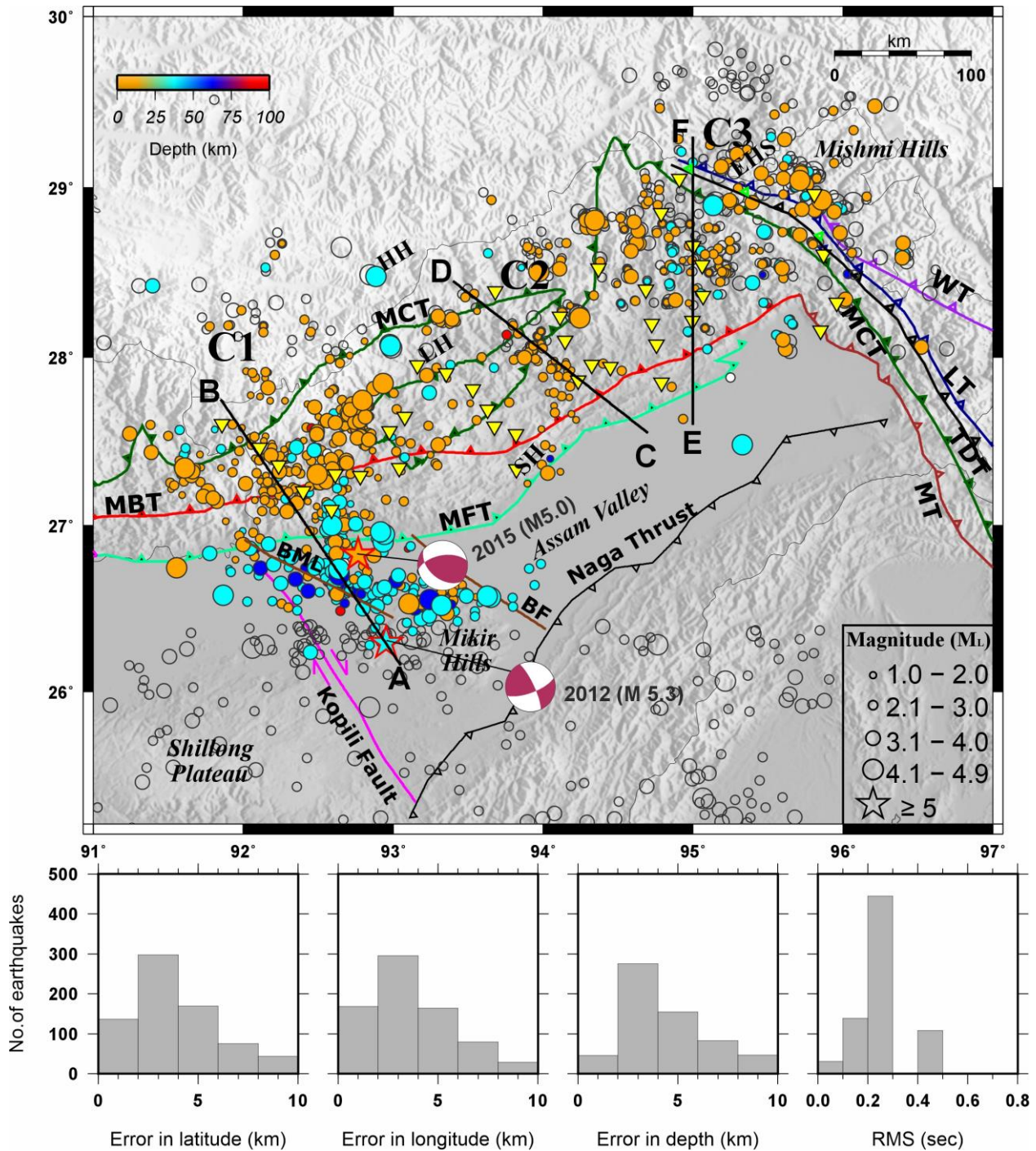


Figure 3. (a) Epicentral distribution of the 806 earthquakes (closed circles) located with an updated 1D velocity model obtained using VELEST. Open circles denote earthquakes which are not used for further analysis. Yellow inverted triangles are broadband seismological stations. Beach balls are the focal mechanism solutions of two earthquakes computed in the present study. The tectonic faults are the same as in Figure 1b. (b) Histograms show errors in hypocenters (km) and time residuals (s).

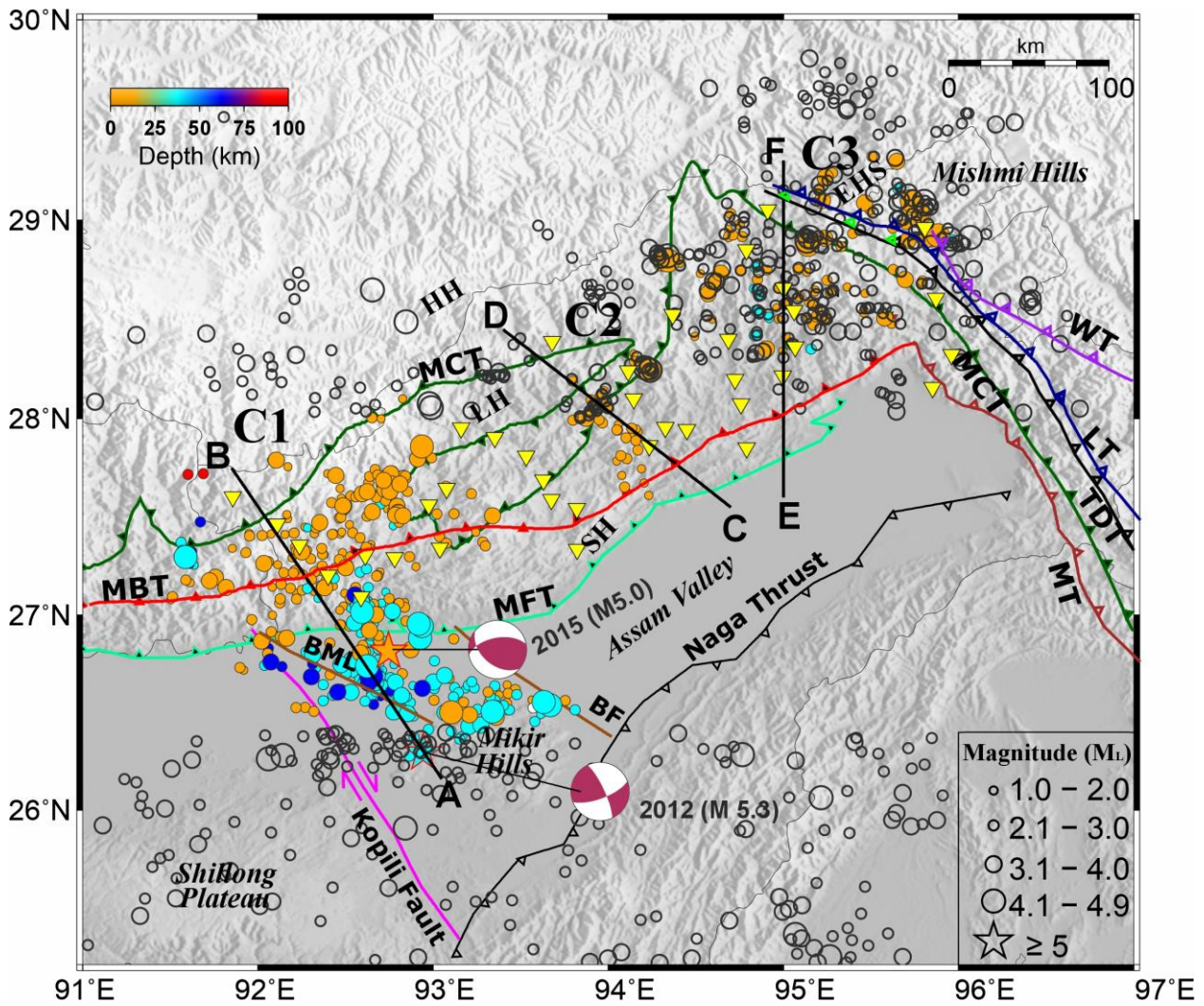


Figure 4. Epicentral distribution of the 540 earthquakes (closed circles) relocated using hypoDD. Open circles denote earthquakes which are not relocated by hypoDD. Other details are the same as in Fig. 3a.

We also determined the focal mechanism solutions of two moderate magnitude earthquakes ($M_L \geq 5.0$, shown as stars in Fig. 3). To determine the moment tensor solutions, we adopted the full waveform inversion scheme in ISOLA code (Sokos and Zahradnik, 2008; 2013). The focal mechanisms of these earthquakes are listed in Table S2 and plotted in Figures 3&4. The match between the synthetic and observed waveform data is shown as an example in Figure S6.

The relocated earthquakes reveal three prominent clusters of seismicity (Figs. 3&4), C1 (Western Arunachal), C2 (Central Arunachal) and C3 (Eastern Arunachal). In general, the seismicity seems to be concentrated mainly in the west (C1) and the syntaxial zone in the east (C3). The central portion of Arunachal (C2) appears less active compared to the adjacent zones (C1 & C3). Depth sections of the single event and hypoDD relocations along three arc normal cross sections (AB, CD and EF as shown in Figs. 3&4) are shown in Figure 5, with error bars. The depth sections derived from both the methods show a similar pattern, except for a few deeper events which are discarded in DD relocations. Seismicity in the depth section along profile CD (Fig.5a) in the central portion indicates that deformation is mainly restricted to the orogenic wedge above the MHT, a scenario typical of the Himalayan arc (Seeber et al., 1981; Ni & Barazangi, 1984). The majority of deeper events in profile AB are to the south of the MFT in the Assam Valley, aligned in the WNW-ESE direction. These deeper earthquakes are attributed to transverse tectonics rather than Himalayan thrusting owing to its proximity to the strike-slip environment. Also, there is no evidence for a significant change in topography in this region. Further, the lateral extent of seismicity indicates a broad zone of deformation. Seismicity along the other profile EF located in the EHS is associated with the NW-SE trending thrust faults (TDT, MT, LT, WT). Even though the majority of earthquakes along this profile occurred in the upper 20 km of the crust, few earthquakes are also found down to 40 km depth along TDT.

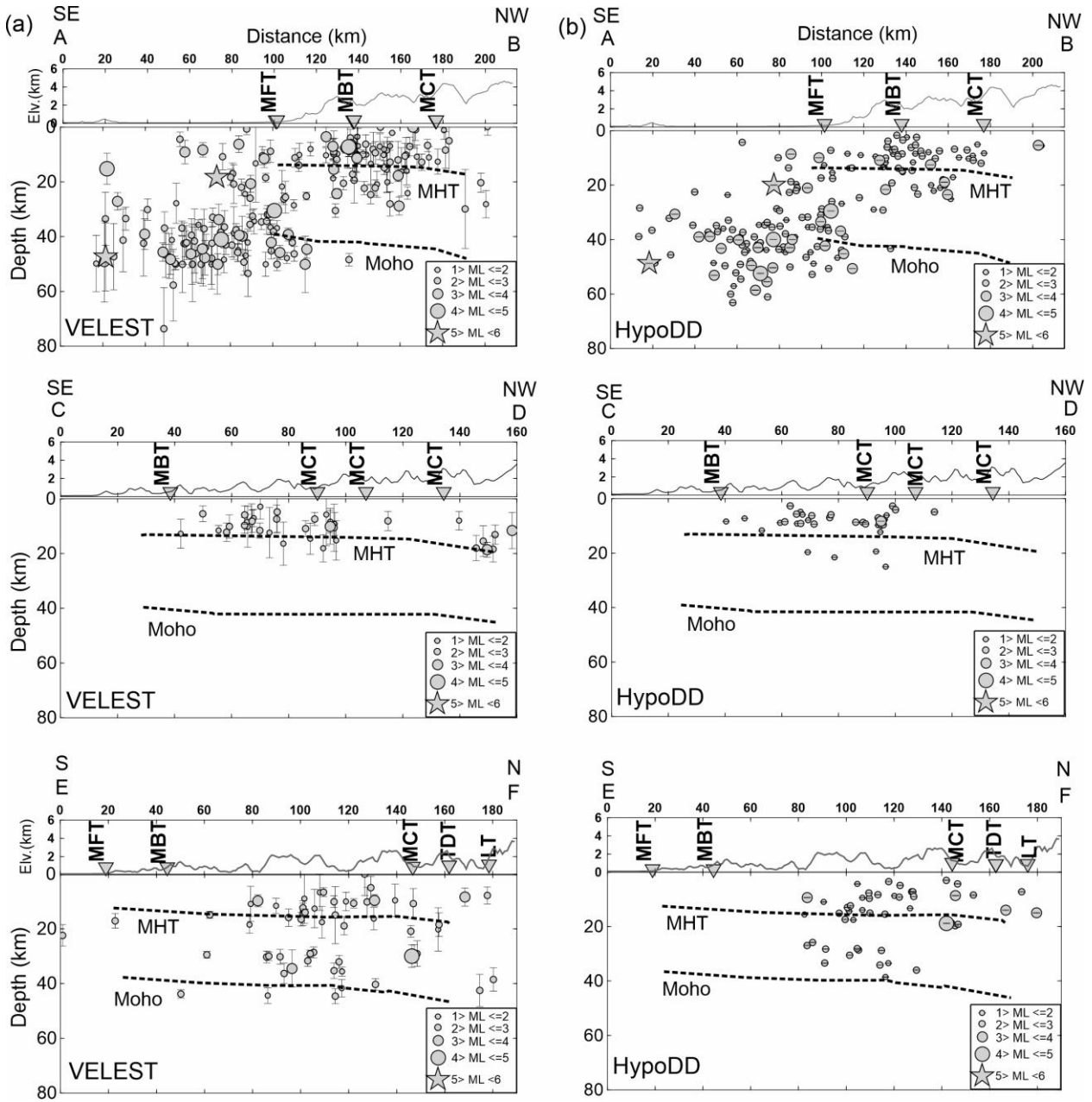


Figure 5. (a) Depth distribution of all the earthquakes located using the single event (VELEST), and (b) double-difference (hypoDD) methods, along profiles AB, CD & EF (Figures 3a, 4a). Closed circles represent earthquakes within 50 km on either side of the profile. The geometry of the MHT and Moho are marked based on the results of receiver function modelling (Singh et al., 2021). The variation of topography and the intersection of major tectonic faults along each profile are shown above each depth section. Error bars indicate the single event (absolute errors) (a) and double difference (relative errors) (b) locations, respectively.

6 3-D velocity tomography

Local earthquake tomography has been carried out to determine the 3D seismic P- wave velocity (V_P) and P- to S- velocity ratio (V_P/V_S) beneath the Arunachal Himalaya. Further, an attempt is made to find a plausible relation between seismicity and crustal velocity structure. The following

criteria have been used to select the data for tomography: (1) an event should have at least 6 P- and 4 S- arrivals, (2) the epicentral distance to the nearest recording station should be less than 150 km, and (c) the travel time residual should not exceed 0.3 s. The selected data set comprises 12,522 picks, which includes 6537 P- and 5985 S- phases from 787 earthquakes (on an average 17 picks/event). We used some out of network events which enable a better resolution of the velocity anomalies at deeper depths (Koulakov, 2009). In the present work, we applied the travel time inversion algorithm SIMUL2000 (Thurber, 1983, 1997; Eberhart-Phillips, 1986), which simultaneously determines hypocentral parameters and 3-D variations in P-wave velocity (V_P) and V_P/V_S by inverting P- arrival and S-P times, using a damped least square inversion.

We define the model space within 26.2–29.5°N, 91.5–96.0°E and 0–60 km (depth range). We use a flexible 3-D grid parameterization with grid nodes having an uneven spacing with linear velocity gradients between the nodes. The initial parametrization is done using the 1-D velocity model obtained with VELEST and a V_P/V_S value of 1.72. The seismic ray path distribution (Fig. S7) shows that the study region is well covered and the ray path density is spatially variable. We performed a number of inversions with variable horizontal (10 km to 50 km) and vertical (3 km to 15 km) grid spacing. Based on resolution parameters and seismic ray path distribution, the final horizontal grid spacing is fixed as 30 km at the centre of the model volume and 40 km for the remaining model space on each plane, at depths of -5, 0, 5, 10, 15, 20, 30, 40, 50 and 60 km. Since the study area is mountainous and a few seismic stations are located at altitudes around 4 km, one layer of the grid is kept at -5 km depth. Empirically determined optimal damping parameters are used (Eberhart-Phillips, 1986). To select the optimal damping value, a trade-off curve between the data and model variances is constructed by performing many one step inversions with the damping parameter values ranging from 25 to 500 (Fig. S8). The final damping value used for inversion is 100. After the inversion, we noticed a variance reduction of 65% for P-arrival time residuals and 55% for the S-P times. The average weighted RMS for travel times decreases from 0.25 s to 0.15 s.

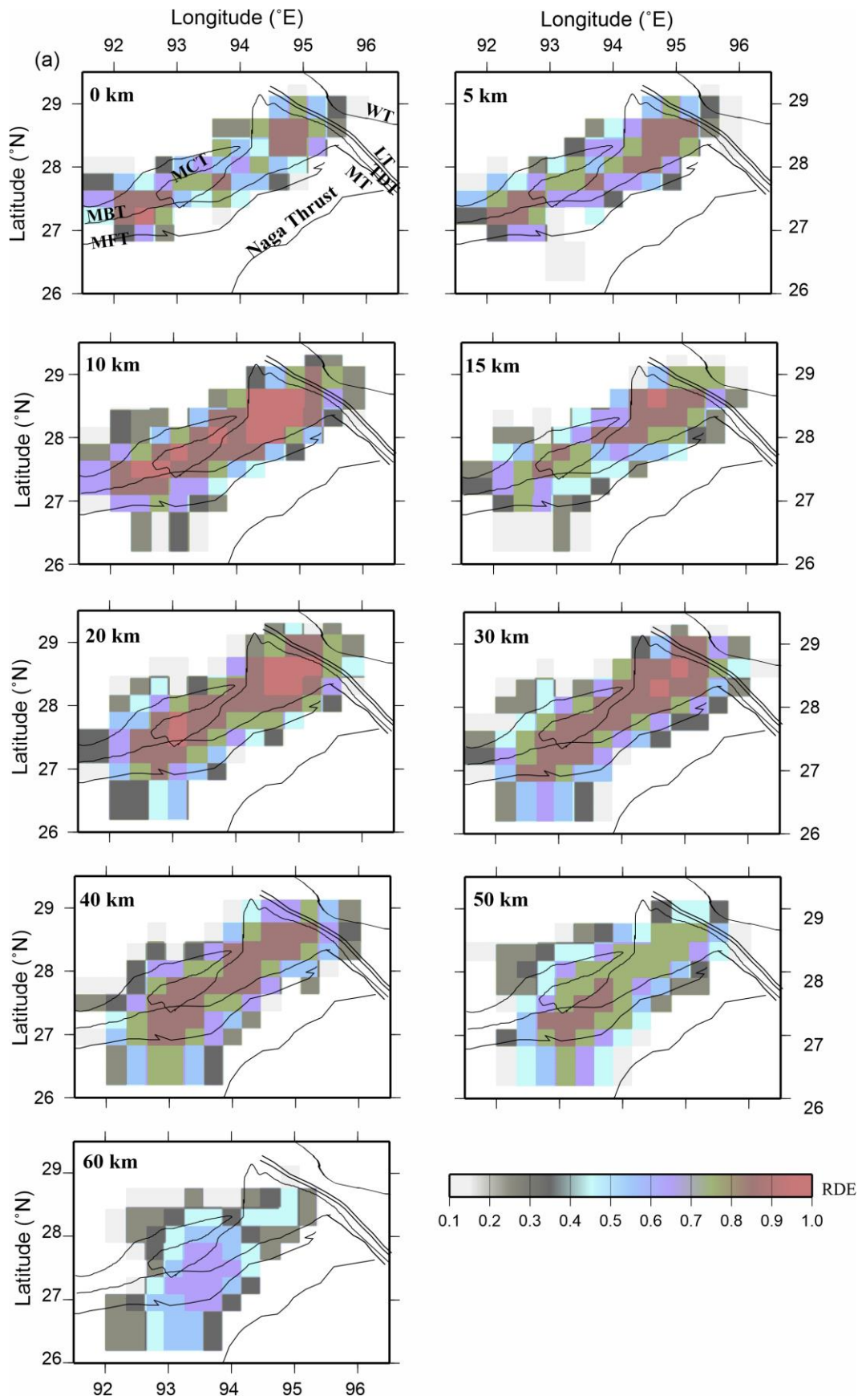
6.1 Assessment of solution quality

This inversion algorithm provides spatial resolution parameters like ray density (KHIT), Derivative Weighted Sum (DWS) and Resolution Diagonal Element (RDE) of the resolution matrix for both V_P and V_P/V_S (Evans et al., 1994). DWS is more representative of the spatial sampling of model space than KHIT (Haslinger et al., 1999). RDE enables the fastest assessment of the solution and indicates the degree of independence of model parameters. The values of RDE for V_P and V_P/V_S are shown in Figure 6. Husen et al. (2004) demonstrated that relatively high (0.5) values of RDE imply a small amount of horizontal smearing. The RDE values (Fig. 6) across our seismic network

reveal that the smearing is small down to 50 km. The distribution of KHIT and DWS for V_P and V_P/V_S (Figs. S9&S10), shows that these model parameters are well constrained at various depths in our study region.

A Checkerboard Resolution Test (CRT) is also carried out to further evaluate the quality of the determined model parameters. We constructed two checkerboard models (Fig. S11), each consisting of alternating high and low anomalies spanning over two grid nodes in the X- and Y- directions. One grid node was left open between the anomalies to test for horizontal velocity smearing. Amplitudes of the input anomalies were set at $\pm 8\%$ for both the V_p and V_p/V_s models. While the anomalies were placed at 5.0, 15.0, 30.0 and 50.0 km depths in the first checkerboard model (Fig. S11a,b), they were placed at 10.0, 20.0, 40.0 and 60.0 km depth in the second. Contrary to the regular checker board models, layers in between were left open to test for vertical smearing.

Along the span of our seismic network (Fig. 1b), the resolution of V_p and V_p/V_s models is good down to 50 km depth. However, major vertical smearing is noticeable between 50.0 and 60.0 km depth (Fig. S11a,c and S11b,d). The recovered results show that the computed V_P & V_P/V_S are well resolved for most of the modelled space down to 50 km depth (Fig. S11). The reliability of the retrieved model can be quantitatively measured by computing the DWS, RDE values and analyzing the checkerboard test. It can be seen from the DWS 500 and RDE 0.2 contours drawn in the checker boards (Fig. S11) that the nodes with $DWS > 500$ and $RDE > 0.2$ are well recovered. Based on these evaluation parameters, we consider that all the nodes with $DWS > 500$, $RDE > 0.2$, are in general well recovered in the checkerboard.



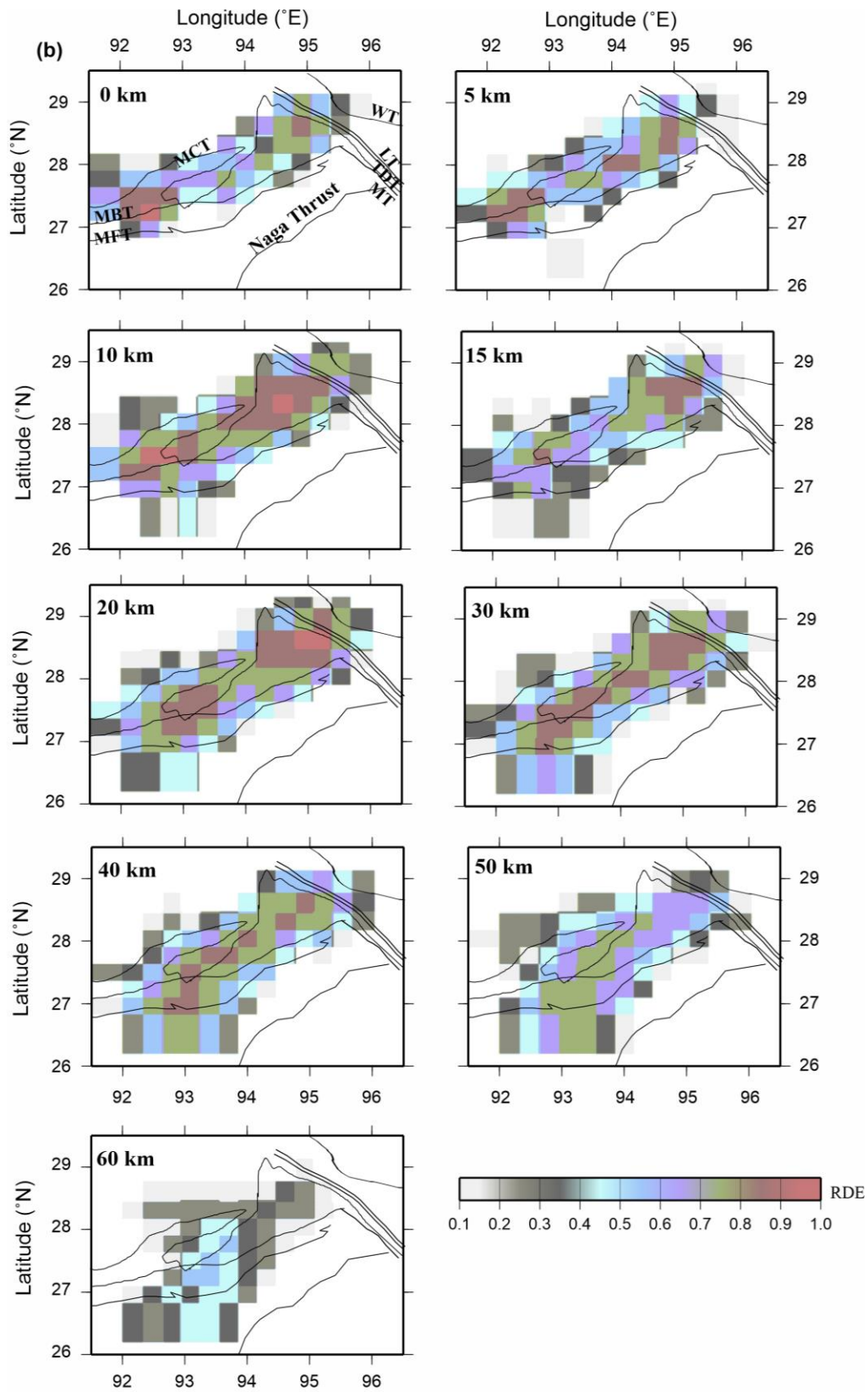


Figure 6. Variation of Resolution Diagonal Element (RDE) at different depths for a) V_p and b) V_p/V_s .

6.2 Tomography Results

Variations in the absolute values of V_P and V_P/V_S in different depth layers reveal small-scale heterogeneities down to 20 km (Figs. 7&8). In general, the absolute values of V_P and V_P/V_S lie in the range of 4.8-8.0 km/s and 1.60-1.85, respectively down to 50 km depth. These images reveal a few pockets of low V_P down to 20 km depth. A horizontal extension of the 6-km-thick low- V_P layer beneath sub-Himalaya is noticed (Fig. 7). Further, to decipher the linkage between crustal structure and earthquake occurrence in the study region, we plotted the absolute values of V_P and V_P/V_S along three vertical cross-sections (I1-I2, J1-J2 and K1-K2 in Fig. 7) across the main subdivisions and major faults of the Himalaya, along profiles where the migrated receiver functions were shown earlier (Singh et al., 2021). Earthquakes within 50 km on either side of the three profiles are superimposed on the velocity images (Figs. 9-11).

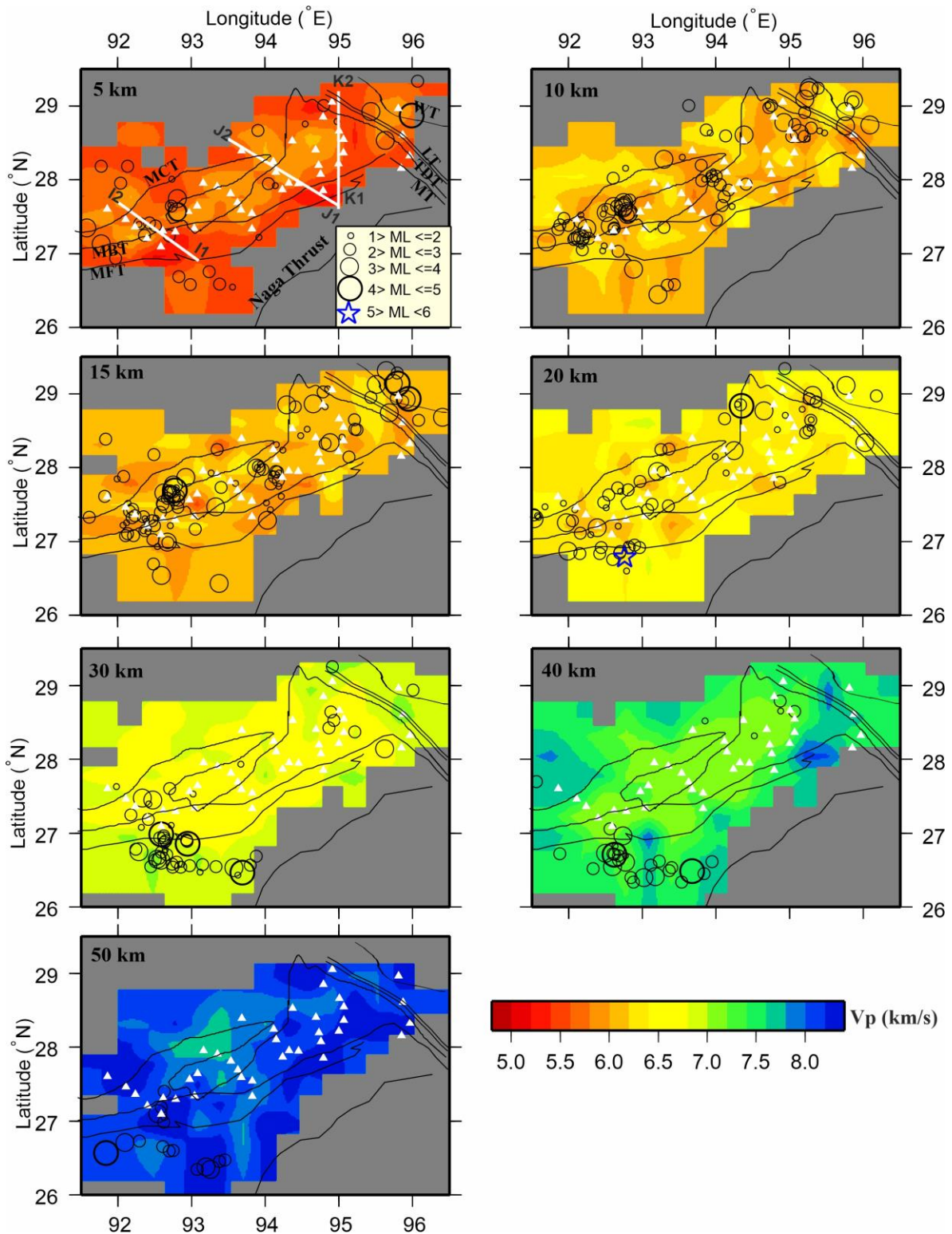


Figure 7. Tomograms of absolute P -wave velocity (V_p). The regions which are not well resolved (DWS < 500 and RDE < 0.2) are masked with gray colour. Open circles denote events that occurred during 2009-2016, within 2 km of each depth slice. White triangles are broadband seismicological stations.

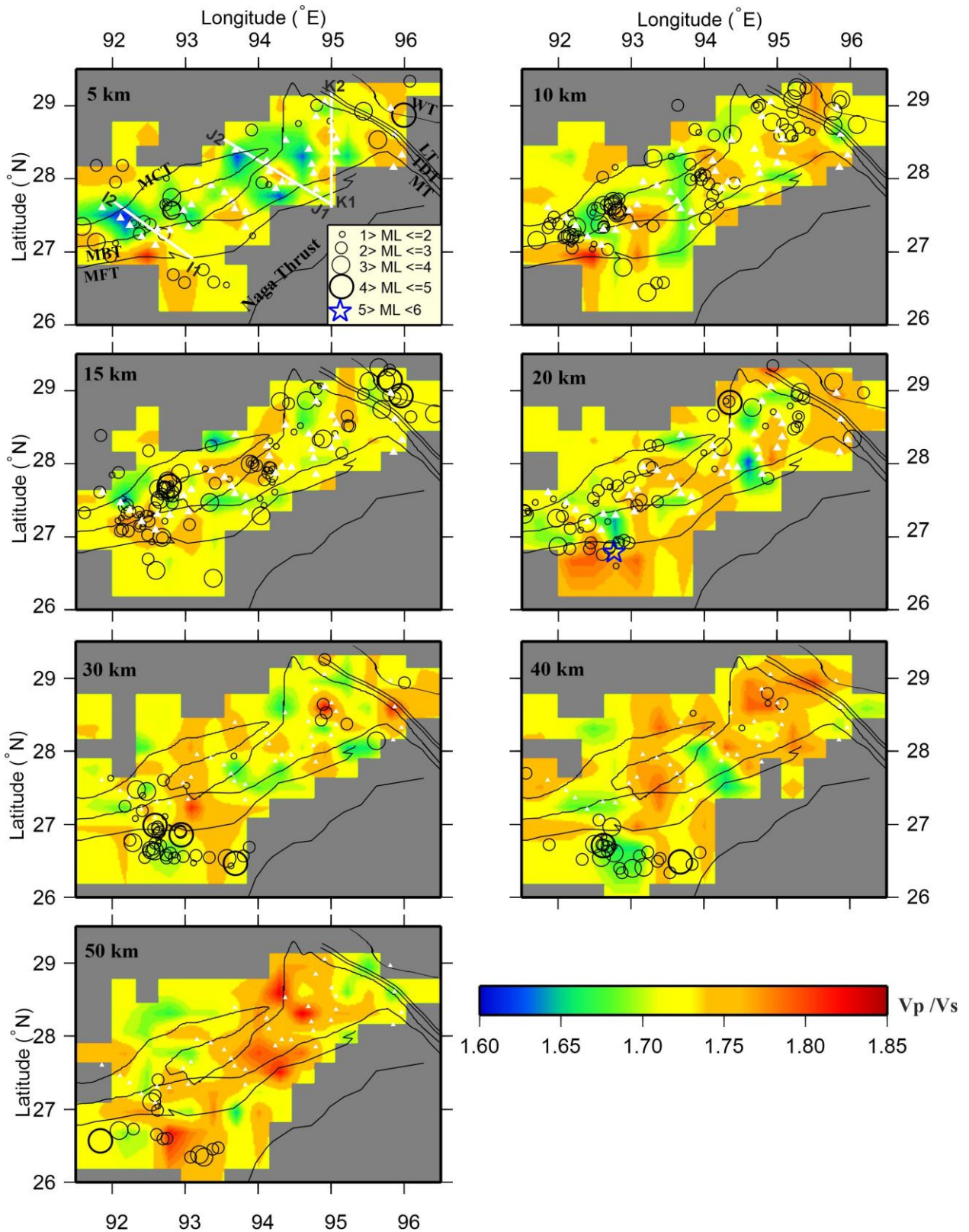


Figure 8. Tomograms of absolute V_p/V_s . The regions which are not well resolved (DWS <500 and RDE <0.2) are masked with gray colour. Open circles denote events that occurred during 2009-2016, within 2 km of each depth slice. White triangles are broadband seismological stations.

Distinct velocity layers in the crust are well identified beneath all the profiles. Overall, the uppermost crust (down to ~10 km depth) beneath Arunachal Himalaya is characterised by V_P values in the range of ~5.6-5.9 km/s and V_P/V_S between ~1.60 and 1.71 (Figs. 9-11). Similar V_P values are noticed in the upper crust of Bhutan (Diehl et al., 2017). The top ~6 km thick layer beneath the sub-Himalaya (SH) between the MFT and MBT (S in Figs. 9-11) has low V_P (~5.2-5.4 km/s) values. Figures 9-11 shows that the upper crust between 10- 20 km has V_P in the range of 5.9 - 6.3km/s and V_P/V_S in the range of 1.65 - 1.72. Velocities in the lower crust to upper most mantle (20- 50 km depth) vary from 6.4 to 8.0 km/s (V_P) and the corresponding V_P/V_S is 1.72-1.85. Although the broad V_P structure remains the same, slight variations are observed in the depth profiles. In spite of the lateral variations, in general, we observed low V_P/V_S values down to mid-crustal (30 km) depths and higher V_P/V_S at lower crustal depths (30-50 km) (Figs. 9-11), except along the western section (I1-I2). Zandt & Ammon (1995) also reported higher V_P/V_S values for the lower crust. We observe low V_P/V_S values (1.60-1.71) in the western section (I1-I2, in Fig. 9). With a slight variation in depth, the obtained velocity variations correspond well with the geometry of the MHT and Moho marked in the migrated receiver function images (Singh et al., 2021). The velocity images show a gently dipping MHT, without significant signatures of a mid-crustal ramp in the Arunachal region. The receiver function results also reveal a simple crust and a gently dipping MHT (Singh et al., 2021). We do not find any specific relation between the distribution of seismicity and velocity variations except in the central Arunachal region. In the central portion of Arunachal, majority of the earthquakes are distributed sub-horizontally in the high V_P/V_S zone (L in Fig. 10) located above the MHT.

Further, to check the reliability of the main features in the tomographic images, we conducted restoring resolution test (RRT) (Zhao et al., 1992) and characteristic test. In the RRT, synthetic phase data is generated with the final derived 3D model as the input model and random errors with a standard deviation of 0.2 s are added to these. This synthetic data is inverted using the same inversion parameters used in the final inversion. The RRT results (Fig. S12) reveal that the main features in the velocity images are well recovered. In the synthetic test, we generate phase data using a synthetic model having a defined anomaly. We find significant anomalies (L & R in Fig. 10b) in the V_P/V_S along profile J1-J2. Therefore, we conduct this test for V_P/V_S along profile J1-J2. We designed the synthetic model using V_P/V_S values between 1.65 and 1.8 in the 5-15 km depth range and used a fixed value of 1.72 for the remaining area (Fig. S13a). After inversion, we noticed that the main features (L & R) were well recovered (Fig. S13b).

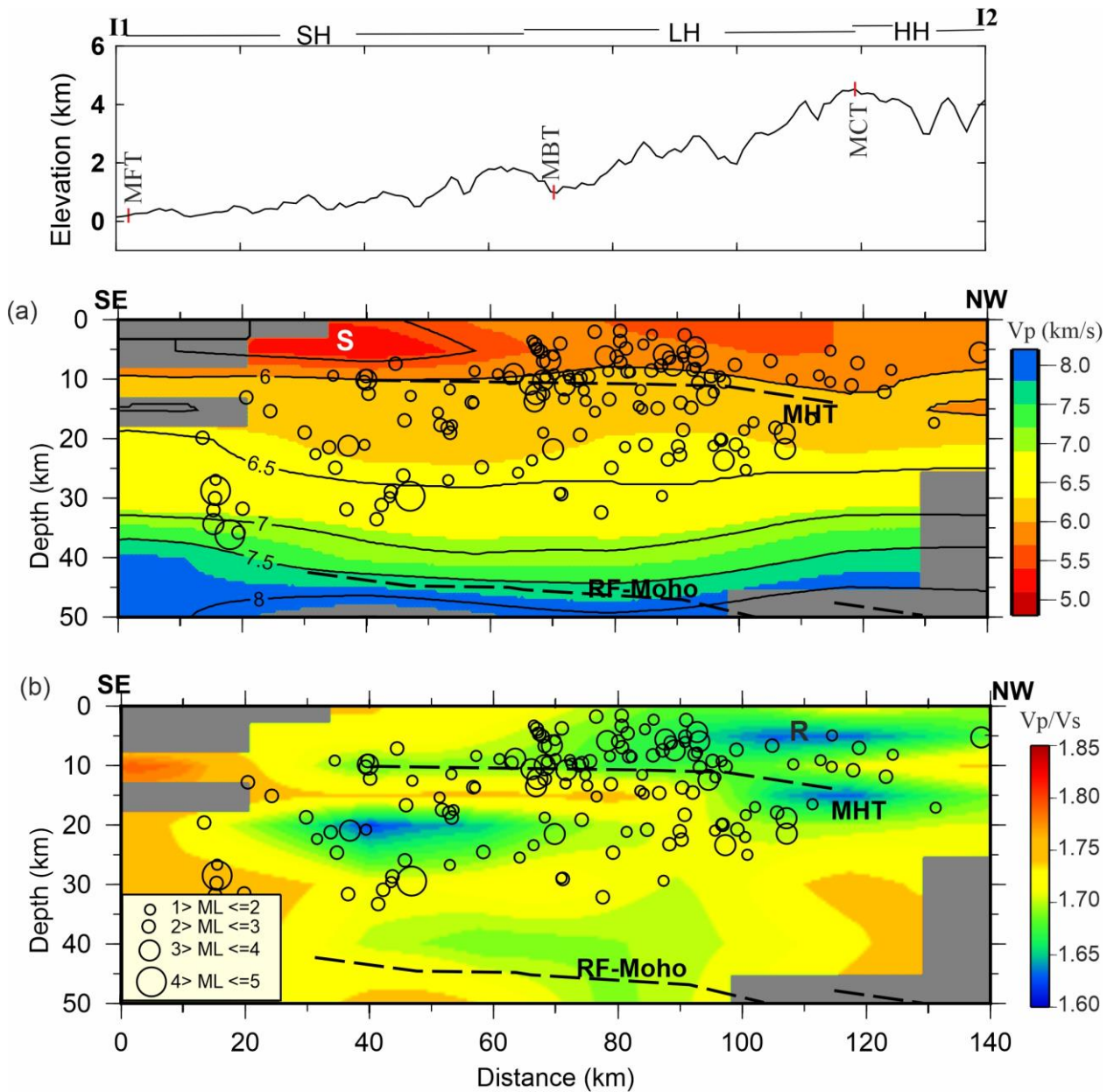


Figure 9. (a, b) Tomographic images of V_p and V_p/V_s along profile I1-I2 (as marked in Fig. 7). Regions which are not well resolved ($DWS < 500$ and $RDE < 0.2$) are masked with gray colour. Open circles represent earthquakes within 50 km on either side of the profile. The geometry of MHT and Moho are marked based on the results from receiver function modelling (Singh et al., 2021). Please see the text for details of the inferred features ('S' and 'R'). Topography variation along the profile is shown on top.

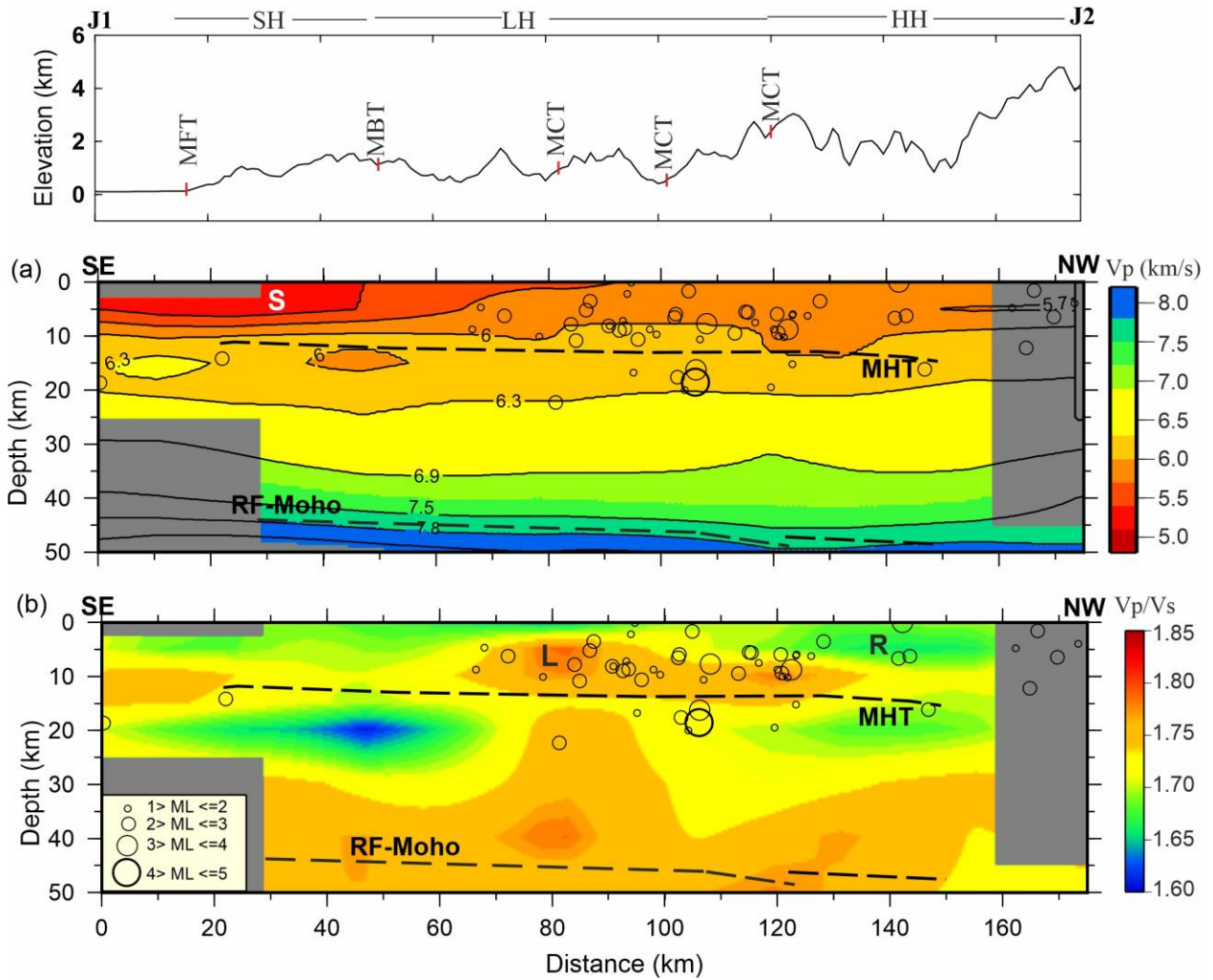


Figure 10. (a, b) Tomographic images of V_p and V_p/V_s along profile J1-J2 (as marked in Fig. 7). Regions which are not well resolved ($DWS < 500$ and $RDE < 0.2$) are masked with gray colour. Open circles represent earthquakes within 50 km on either side of the profile. Please see the text for details of the inferred features ('S', 'R' and 'L'). Other details are the same as in Fig. 9.

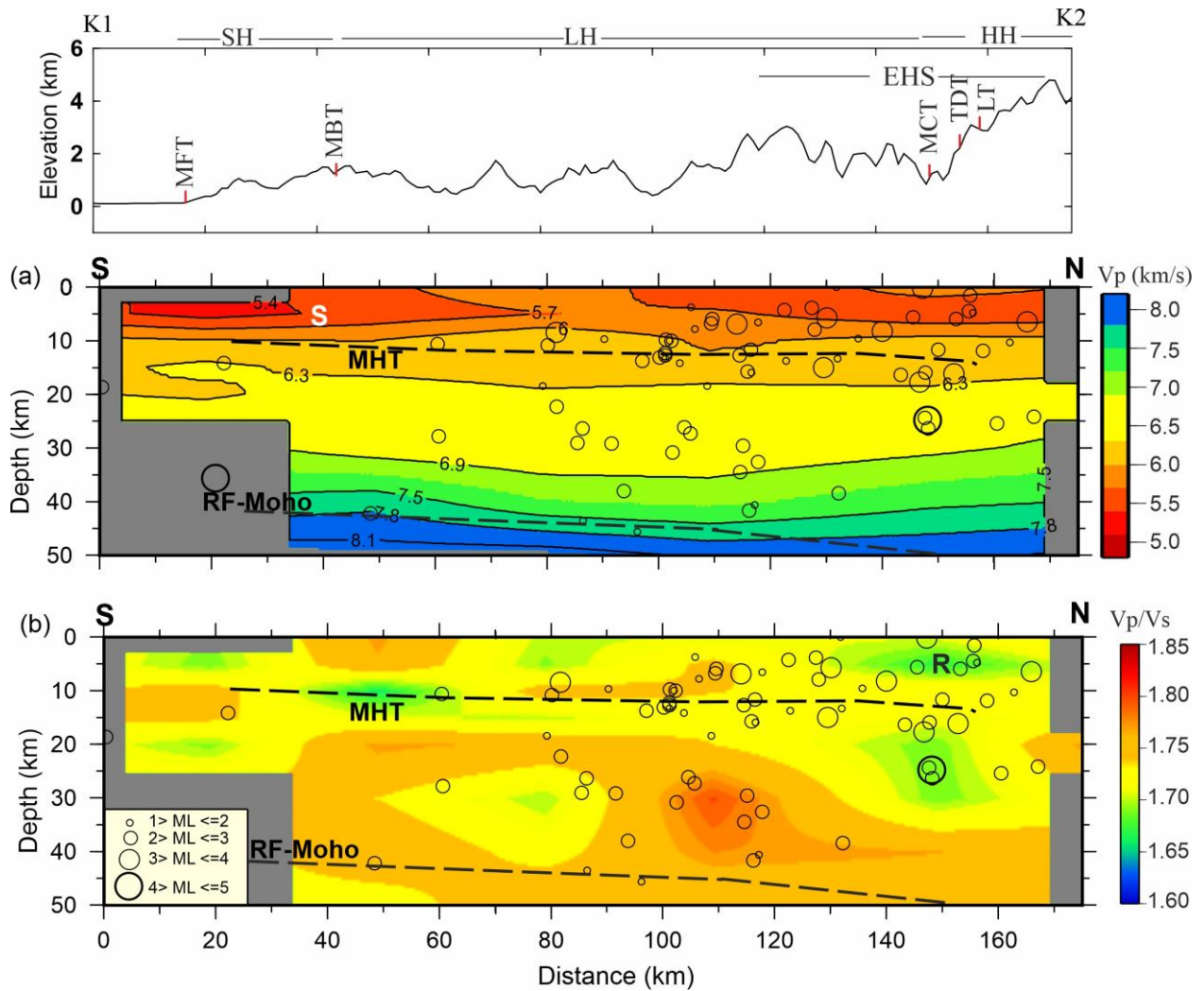


Figure 11. (a, b) Tomographic images of V_p and V_p/V_s along profile K1-K2 (as marked in Fig. 7). Regions which are not well resolved ($DWS < 500$ and $RDE < 0.2$) are masked with gray colour. Open circles represent earthquakes within 50 km on either side of the profile. Please see the text for details of the inferred features ('S' and 'R'). Other details are the same as in Fig. 9.

7 Discussion

7.1 Seismicity

The seismotectonic regime in the Arunachal Himalaya seems to be very complex and is summarized in Figure 12. The central portion (C2 in Figs. 3, 4 & 12) appears less active in terms of instrumental seismicity ($M_c = 2.2$) compared to the adjacent regions (C1 & C3), over 7 years of our recording period (2009 December to 2016 March). Most of the local seismicity is concentrated in the western and eastern zones (C1 & C3 in Figs. 3 & 4). As reported by Diehl et al. (2017) in the Bhutan Himalaya, the observed seismicity extends far south of the major Himalayan thrust faults in western Arunachal, where seismicity extends to south of the Mikir Massif (C1 in Figs. 3 & 4). The NW-SE trending KF and BF are the major reported faults in the foreland (Nandy, 2001; Bhattacharya et al., 2008; Kayal et al., 2012). Further, the earthquakes are not just clustered close to KF, but are spread

~100 km on either side, indicating a broad deformation zone. However the observed seismicity north of the Kopili fault zone (KFZ) in the foreland is distributed in the WNW-ESE direction, conjugate to KF. To confirm the distribution of seismicity in the foreland, we also compared our earthquake catalog with the regional catalog prepared based on data from the Indian National Network operated by National Center for Seismology (NCS) and USGS catalog (Fig. S14). The NCS epicenters indicate similar, E-W strike of that cluster (but offset by about 40 km to the south). Rakshit and Rakshit (2022) reported that the WNW-ESE trending Bhairabkunda-Mazbat Lineament (BML) to the north of KFZ is seismically active and it may be the causative fault for the 28th April, 2021 Mw 6.0 earthquake in this region (Fig. 12). Rakshit and Rakshit (2022) also argued for a strike-slip nature of the KF and differential stress conditions due to the various stress zones present adjacent to the KFZ, like the (most dominant) Shillong Plateau, in the west and the relatively less seismically active Assam Valley in the east (Angelier and Baruah, 2009). These could also indicate transverse features in the region, such as the BML. The present study also shows that seismicity to the north of KFZ is associated with BML, which is conjugate to KF. In other regions of Arunachal, the seismicity (C2 & C3) lies between MBT and MCT. Focal depths of majority of earthquakes in the Assam valley are located in the Indian lower crust (35-50 km) and the depths decrease to 25 km, mostly above the MHT, beneath the Himalaya (as shown along profile AB in Fig. 5b).

Based on seismicity and moment tensor solutions, Diehl et al. (2017) reported that the dextral DCF, a feature that potentially marks the western boundary of the Shillong block, might cut across the MHT between Nepal and Bhutan. Similarly, previous studies (Bhattacharya et al., 2008, 2010; Kayal et al., 2006, 2010;2012; Vernant et al., 2014) proposed that KF extends into the Himalaya up to the MCT and is capable of generating M7 earthquakes in the eastern Himalaya and the Foreland basin. To examine the nature of faulting in the study region and to examine the possibility of continuation of KF into the Himalaya, we studied the moment tensor solutions (Fig. 12) determined in the present study, from regional data (Kayal et al., 2012) and those from the global catalog (gCMT). The moment tensor solutions of earthquakes computed in the present study reveal that the earthquake (M5.1, 2015) located just south of the MFT (at a shallow depth of 17 km) has a thrust mechanism and the deeper event (M5.3, 2012) (45 km focal depth) located east of KF is a strike-slip (Fig. 12). The largest recent event (Mw6.0 2021) to the north of KFZ in the foreland (shown in Figure 12), is associated with a strike slip mechanism. The M6.1 2009 earthquake in the Himalaya has a thrust mechanism (Fig. 12). The seismicity distribution & focal mechanism solutions in the western Arunachal inferred from the present study and global catalogs cannot unambiguously resolve the continuation of KF into Himalaya.

However, the foreland seismicity seems to be associated with a strike slip regime, as also revealed by the moment tensor solution of the 2012 M5.3 earthquake computed in this study and other earthquakes from global catalogs (Fig. 12). The strike of one of the nodal planes of the Mw6.0 2021 earthquake which is located in our observed seismicity cluster (Fig. 12) matches with the WNW-ESE strike of the seismicity distribution. This prompts us to postulate that the seismicity in the foreland is associated with the WNW-ESE oriented fault/shear zone in the Indian crust, probably BML, that is conjugate to the KF. The dense seismic network in the Assam valley and further geological studies can throw better light on this newly identified fault.

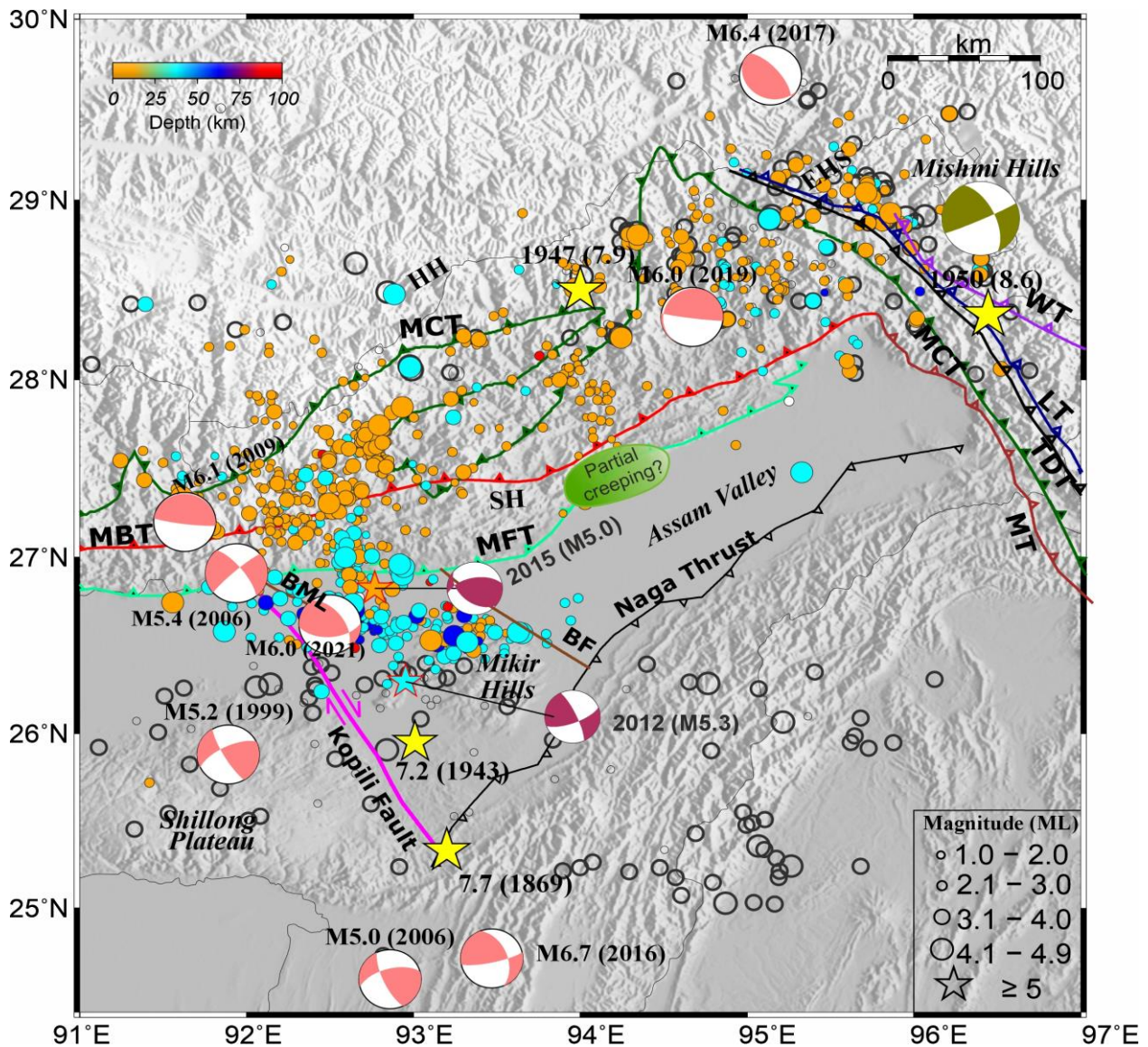


Figure 12. Seismotectonic scenario of the Arunachal Himalaya. Closed circles indicate earthquakes with magnitudes $\geq M_c$ located in the present study. The focal mechanisms are taken from the gCMT catalog (Pink beach balls), present study (Purple beach balls) and the 1950 earthquake (dark green beach ball) (Ben-Menahem et al., 1974). The locations of M 7.7 (1869) and M 7.2 (1943) earthquakes are taken from Kayal et. al (2012).

In central Arunachal, seismicity follows the general trend of earthquakes along the Himalayan arc with deformation limited to a depth of 20 km, above the MHT. Most of the seismicity is sub-horizontal between MBT and MCT. However, we also noticed a few earthquakes in the sub-Himalaya between MBT & MFT and a small cluster of earthquakes north of MCT in the Higher Himalaya, in the vicinity of 1947 earthquake (Fig. 12). During our recording period, we have recorded only one earthquake of $M_L > 4.0$, four of $M_L > 3.0$ & < 4 and all the remaining earthquakes have magnitudes < 3.0 . The relatively lower seismicity in central Arunachal Himalaya is also apparently observed in the global catalogs (Fig. 1b, Fig. S14). Also, Rajendran & Rajendran, (2011) reported low seismicity between the Mikir Hills and Mishmi Thrust. The convergence rates derived from GPS are also not well defined in this segment and therefore not conclusive to explain the low seismicity. This region is the only segment of the Himalayan arc with no known big event and the smallest level of interseismic coupling (Hetényi, et al., 2016b; Stevens & Avouac, 2016). The Mw 7.7 (1947) earthquake in the north central part of Arunachal was insufficient to rupture the entire MHT and might have occurred on an out-of-sequence thrust (Chen & Molnar, 1977). The low seismicity may either be due to a fully locked zone with strain accumulation, low deformation or aseismic slip in this part of Arunachal Himalaya. Further, Cattin & Avouac, (2000) suggested that the strain accumulation in the interseismic period results in small to moderate sized earthquakes in the downdip verge of the MHT in the lesser Himalaya of Nepal and very low to no seismicity in the updip region. The mid-crustal seismicity clusters associated with the locked zones in the down dip edge of the MHT are well known in the Nepal, Garhwal and Bhutan Himalaya (Monsalve et al., 2006; Mahesh et al., 2013; Diehl et al., 2017). In western Bhutan, the observed seismicity cluster in the Higher Himalayan front was correlated with the 3500 m topography contour and locked to creep transition, indicating stress build-up along a fully locked MHT (Diehl, et al., 2017). Similar models were also proposed for the observed seismicity clusters in the high Himalayan seismic belt of Nepal and northwestern Himalaya (Cattin & Avouac, 2000; Paul et al., 2001; Bollinger et al., 2004). With the existing data, we find a small cluster at mid-crustal levels along the down dip part of MHT beneath the higher Himalaya (Fig. 5a) and the seismicity is even lower than that in the adjoining Himalayan regions. Receiver function (Singh et al., 2021) and tomography images along with seismicity patterns, reveal a flat seismogenic portion of the MHT between 70 and 130 km north of the MFT (Fig. 10b) in this region (Fig. 10). Diehl et al. (2017) also observed a flat, seismogenic MHT in eastern Bhutan, abetting our study region in the west. On the basis of slip rates computed from GPS (Marechal et al., 2016), they related the flat seismogenic MHT to a partially creeping segment or to increased background seismicity. In the Arunachal region, the GPS data is very sparse and there are no slip rate models available to constrain the results. In view of the smallest level of interseismic coupling in this region (Stevens & Avouac, 2016), we hypothesize

that the observed ~60 km long flat seismogenic part of the MHT might be correlated with a partial creeping segment. The stress redistribution throughout the seismic cycle may lead to a creeping segment that is slipping at rates smaller or larger than the long-term rate (Avouac, 2015). Avouac (2015) described the favorable factors which enable creep in terms of “fluid pressure, temperature, chemical environment, fault geometry and sudden stress changes from nearby earthquakes”. In the next section, we will discuss about fluids along the MHT near the assumed partial creeping segment. The creeping faults or a segment of the fault which is creeping slowly can still produce a large earthquake similar to locked faults (Harris, 2017; Chen & Bürgmann, 2017). The slip rate models derived from GPS data in this segment can provide better information regarding the proposed partial creeping hypothesis. Whether or not the imaged seismogenic segment is related to a partially creeping MHT, the central Arunachal region, which is in the seismic gap can host M8 earthquakes.

The syntaxial zone in the east is the other sector where earthquakes cluster. The area of Mishmi Massif to the east of Arunachal Himalaya is host to a number of NW-SE trending thrust faults. This region is tectonically and geologically complex, owing to a triple junction. The region also experienced many aftershocks of the 1950 Assam earthquake, suggesting rejuvenation of neo-tectonic activities in the area, even far away from the region of the mainshock (Poddar, 1950). The current analysis shows that very few earthquakes are located in the vicinity of the 1950 earthquake and southeast of it, indicating that the southeastern part of Mishmi and Lohith thrusts may not be currently very active. The shortening rates computed from GPS get smaller from the NW to SE parts of the Mishmi and Lohith thrusts, indicating a locked portion of these faults, which was activated during the 1950 earthquake (Gupta et al., 2015). The entire crust is seismically active in the EHS region. Kundu et al. (2020) and Yadav et al. (2021) also reported that earthquakes in this region are deeper down to 40 km.

7.2 Crustal structure, geometry of the MHT and Moho

In the sub-Himalaya, the uppermost crust (0-6 km depth) has low V_P (~5.2-5.4 km/s) values (S in Figs. 9-11), indicating sediments. The velocity reduction (at shallow depths) may result from a combination of various factors such as large sediment thickness, high pore-pressure and active strain. The low V_P/V_S below the surface trace of the MCT (R in Figs. 9-11) might be a signature of felsic migmatites, kyanite-bearing paragneiss and leucogranite in the upper crust, as correlated with surface geology of western Arunachal (Gururajan & Choudhary 2003; Yin et al., 2010; DeCelles et al., 2016). The general occurrence of rocks such as quartzites, quartz arenite, phyllites, granitic augen orthogneiss and schists (Yin et al., 2010; Webb et al., 2013; DeCelles et al., 2016) in the upper crust also supports a felsic crust in this region. Further, laboratory based studies indicate that the quartzite and quartz dominated metamorphic rocks have low V_P/V_S values (Christensen, 1996). A similar kind

of low V_P/V_S has also been reported for the upper crust beneath the Bhutan Himalaya (Singer et al., 2017b) and upper and middle crust below the Higher Himalaya in eastern Nepal and southern Tibet (Monsalve et al., 2008).

Along the western profile, majority of the seismicity is located within 20 km of the crust and low V_P/V_S values (1.60-1.71) are noticed in the entire crust (Fig. 9). Low values in the mid to lower crustal levels may be due to high porosity, presence of fluids (or gas) (Kaypak, 2008) and anisotropy (Wang et al., 2009). Due to high lithostatic pressure in the deeper part of the crust, high pore pressure is required to maintain high porosity, which is unlikely. Wang et al. (2009) have shown that 5% of P- and S-wave anisotropy is sufficient to change an average V_P/V_S value of 1.78 for continental crust (Zandt & Ammon, 1995), making it an important factor while interpreting the crustal composition using V_P/V_S values. Singh et al. (2021) presented evidence for anisotropy at mid- to lower crustal levels beneath the Arunachal region, which is especially stronger along this profile. Hence, the observed low V_P/V_S values down to lower crustal levels can be attributed to anisotropy in the mid-to-lower crustal depths. Anisotropy at mid-crustal depths is also reported from other segments of the Himalaya (Singh et al., 2010; Schulte-Pelkum et al., 2005; Nábělek et al., 2009; Singer, et al., 2017b).

In the central Arunachal region, the imaged velocity structure along with seismicity, reveals a gently dipping MHT (Fig. 10). We do not observe any signatures of a sharp mid-crustal ramp in this region and the crustal structure seems to be less complex compared to the adjacent Himalayan regions. The obtained velocity variations/anomalies correlate well with the geometry of the MHT and Moho mapped using Receiver Functions (Singh et al., 2021). The geometry of the MHT is not clear in the western (I1-I2) and eastern (K1-K2) sections as also observed by Singh et al. (2021). We find that most of the seismicity is sub-horizontal between MBT and MCT and located above a flat portion of the MHT, lying in a high V_P/V_S zone (L in Fig. 10). The observed sub-horizontal high V_P/V_S zone extends ~70- and 130- km north of the MFT, between 7-13 km depth. The high V_P/V_S is due to a low velocity zone (LVZ) in that depth range. A LVZ along the MHT was also observed in Nepal Himalaya (Nábělek et al., 2009; Duputel et al., 2016; Subedi, et al., 2018), Garhwal Himalaya (Caldwell et al., 2013, Gupta et al., 2022) and northwest Himalaya (Hazarika et al., 2017). The observed LVZ above the MHT is due to possible presence of fluids (partial melt, aqueous fluids or both) resulting from metamorphic dehydration of the underthrusting Indian plate below the MHT. The presence of fluids may enable creep (Avoc, 2015) along this segment of MHT.

Along the eastern profile, the entire crust is seismically active (Fig. 11). The moderate to high V_P (5.4-5.7) and low to moderate V_P/V_S (1.69 – 1.71) values in the uppermost crust (0-6 km depth)

beneath the Eastern Himalayan Synaxis might be signatures of Mishmi crystalline and ophiolitic mélangé mainly comprising garnetiferous metavolcanics, marble bands, and graphitic-garnet schist, as correlated with the complex surface geology of EHS (Gururajan & Choudhary 2003). The high V_P/V_S values below the MHT represent the underlying Indian lower crustal material (Zandt & Ammon, 1995). Pockets of low V_P/V_S values down to mid-crustal levels are due to anisotropy at these depths (Singh et al., 2021). The V_P/V_S for most of the crust is less than 1.78, a value that corresponds to a Poisson solid. Thus, it signifies that the entire crust behaves in a rigid manner and is capable of accumulating strain energy which can be released to produce earthquakes throughout the crust.

8 Conclusions

The present study provides the first detailed information about seismicity and 3-D velocity structure of Arunachal Himalaya, using earthquake data recorded by a dense seismic network of 41 broadband stations operated during December 2009 to March 2016. A total of 1418 earthquakes having magnitudes in the range of ML 1.0 to 5.2 are located during the recording period. The western Arunachal region and the syntaxial zone in the east are seismically active compared to the central Arunachal portion. The seismicity in western Arunachal extends to south of the Mikir Hills in the Foreland. In the 0-50 km depth range, the absolute V_P and V_P/V_S values vary between 4.8-8.2 km/s and 1.60-1.85, respectively. The seismic images exhibit signatures of sediments in the sub-Himalayas. The low V_P/V_S in the mid-to-lower crustal depths can be associated with crustal anisotropy. The velocity images along with seismicity reveal a gently dipping seismogenic MHT in central Arunachal. The ~ 60 km long seismogenic flat portion of the MHT in the central Arunachal region might be related to a partial creeping segment.

Acknowledgments

The broadband seismic stations were operated under the GENIAS project of CSIR-NGRI. This work is performed under the FBR-005(MRK) project. The authors thank their corresponding institutes for support. The authors thank Dr. Charu Kamra for helping in computing the focal mechanism solutions. All the figures are made with the Generic Mapping Tools (Wessel and Smith, 1998). The authors thank the Editor and two anonymous reviewers for their constructive comments that improved the manuscript.

References

Angelier, J., & Baruah, S. (2009). Seismotectonics of northeast India: a stress analysis of focal mechanism solutions of earthquakes and its kinematic implications. *Geophys J Int.* 178(1):303–326.

- Avouac, J.-P. (2015). From geodetic imaging of seismic and aseismic fault slip to dynamic modeling of the seismic cycle. *Annual Review of Earth and Planetary Sciences*, 43, 233–271, doi:10.1146/annurev-earth-060614-105302.
- Avouac, J. P., Meng, L., Wei, S., Wang, T., & Ampuero, J. P. (2015). Lower edge of locked Main Himalayan Thrust unzipped by the 2015 Gorkha earthquake. *Nature Geoscience*, 8(9), 708-711. <https://doi.org/10.1038/ngeo2518>.
- Barman, P., Jade, S., Shringeshwara, T.S., Kumar, A. Bhattacharya, S., Ray, J., Jagannathan, S., & Jamir, W.M. (2017). Crustal deformation rates in Assam Valley, Shillong Plateau, Eastern Himalaya, and Indo-Burmese region from 11 years (2002–2013) of GPS measurements. *International Journal of Earth Sciences (Geol Rundsch)*, 106:2025–2038.
- Ben-Menahem, A., Aboodi, E., & Schild, R. (1974). The source of the great Assam earthquake-an interplate wedge motion. *Physics of the Earth and Planetary Interiors*, 9 (4), 265-289.
- Bhattacharya, P.M., Mukhopadhyay, S., Majumdar, R.K., & Kayal, J.R.(2008). 3-D seismic structure of the Northeast India region and its implications for local and regional tectonics. *Journal of Asian Earth Sciences*, 33, 25–41
- Bhattacharya, P.M., Kayal, J.R., Baruah, S., & Arefiev, S.S. (2010). Earthquake Source Zones in Northeast India: Seismic Tomography, Fractal Dimension and b Value Mapping. *Pure and Applied Geophysics*, 167, 999-1012. <https://doi.org/10.1007/s00024-010-0084-2>
- Bilham, R. (2019). Himalayan earthquakes: a review of historical seismicity and early 21st century slip potential. *Geological Society, London, Special Publications*, 483(1):423.
- Bilham, R., & England, P. (2001). Plateau ‘pop-up’ in the great 1897 Assam earthquake. *Nature*, 410(6830), 806-809.
- Bollinger, L., Avouac, J.P., Cattin, R., & Pandey, M.R. (2004). Stress buildup in the Himalaya. *Journal of Geophysical Research*, 109, B11405. <http://dx.doi.org/10.1029/2003JB002911>.
- Caldwell, W. B., Klemperer, S. L., Lawrence, J. F., & Rai, S. S. (2013). Characterizing the Main Himalayan Thrust in the Garhwal Himalaya, India with receiver function CCP stacking. *Earth and Planetary Science Letters*, 367, 15–27. <https://doi.org/10.1016/j.epsl.2013.02.009>.
- Cattin, R., & Avouac, J.P. (2000). Modeling mountain building and the seismic cycle in the Himalaya of Nepal. *Journal of Geophysical Research: Solid Earth*, 105 (B6), 13,389–13,407. <http://dx.doi.org/10.1029/2000JB900032>
- Chen W.-P., & Molnar, P. (1977). Seismic moments of major earthquakes and the average rate of slip in central Asia. *Journal of Geophysical Research*, 82, 2945-2969.
- Chen, W. P., & Molnar, P. (1990). Source parameters of earthquakes and intraplate deformation beneath the Shillong Plateau and the northern Indoburman ranges. *Journal of Geophysical Research: Solid Earth*, 95(B8), 12527-12552.
- Chen, K. H., & Bürgmann, R. (2017). Creeping faults: Good news, bad news?. *Reviews of Geophysics*, 55, 282–286, doi:10.1002/2017RG000565.

- Christensen, N.I. (1996). Poisson's ratio and crustal seismology. *Journal of Geophysical Research*, 101, 3139–3156.
- Dal Zilio, L., van Dinther, Y., Gerya, T., & Avouac, J. P. (2019). Bimodal seismicity in the Himalaya controlled by fault friction and geometry. *Nature communications*, 10(1), 1-11.
- De, R., & Kayal, J. R. (1990). Crustal P-wave velocity and velocity-ratio study in northeast India by a microearthquake survey. *Pure and Applied Geophysics*, 134(1), 93-108.
- DeCelles, P. G., Carrapa, B., Gehrels, G. E., Chakraborty, T., & Ghosh, P. (2016). Along-strike continuity of structure, stratigraphy, and kinematic history in the Himalayan thrust belt: The view from Northeastern India. *Tectonics*, 35 (12), 2995-3027. doi: 10.1002/2016TC004298
- Diehl, T., Singer, J., Hetényi, G., Grujic, D., Clinton, J., Giardini, D., Kissling E., & GANSSER Working Group GANSSER Working Group. (2017). Seismotectonics of Bhutan: Evidence for segmentation of the Eastern Himalayas and link to foreland deformation. *Earth and Planetary Science Letters*, 471, 54-64.
- Duputel, Z., Vergne, J., Rivera, L., Wittlinger, G., Farra, V., & Hetényi, G. (2016). The 2015 Gorkha earthquake: A large event illuminating the Main Himalayan Thrust fault. *Geophysical Research Letters*, 43, 2517–2525. <https://doi.org/10.1002/2016GL068083>.
- Eberhart-Phillips, D. (1986). Three-dimensional velocity structure in northern California coast ranges from inversion of local earthquakes. *Bulletin of the Seismological Society of America*, 76, 1025–1052.
- Evans, J.R., Eberhart-Phillips, D., & Thurber, C.H. (1994). User's manual for SIMULPS12 for imaging V_p and V_p/V_s : a derivative of the “Thurber” tomographic inversion SIMUL3 for local earthquakes and explosions. *Open-file Report 94-431*. U.S. Geological Survey, 101 pp.
- Gansser, A. (1964). *Geology of the Himalayas*. Wiley Eastern Limited.
- Gururajan, N.S., Choudhuri, B.K. (2003). Geology and tectonic history of the GuptaLohit Valley, Eastern Arunachal Pradesh. *J. Asian Earth Sci.* 21 (7), 731–741.
- Gupta, S., Mahesh, P., Nagaraju, K., Sivaram, K., & Paul, A. (2022). 3-D seismic velocity structure of the Kumaun–Garhwal (Central) Himalaya: insight into the Main Himalayan Thrust and earthquake occurrence. *Geophysical Journal International*, 229, 138–149. <https://doi.org/10.1093/gji/ggab449>
- Gupta, H. K. (1984). Seismicity in the vicinity of dams on Himalayan rivers and the problem of reservoir induced earthquakes. *Journal of Geological Society of India (Online archive from Vol 1 to Vol 78)*, 25(2), 85-93.
- Gupta, T. D., Riguzzi, F., Dasgupta, S., Mukhopadhyay, B., Roy, S., & Sharma, S. (2015). Kinematics and strain rates of the Eastern Himalayan Syntaxis from new GPS campaigns in Northeast India. *Tectonophysics*, 655, 15-26.
- Harris, R. A. (2017). Large earthquakes and creeping faults. *Reviews of Geophysics*, 55, 169-198, doi:10.1002/2016RG000539.
- Haslinger, F., Kissling, E., Ansorge, J., Hatzfeld, D., Papadimitriou, E., Karakostas, V., Makropoulos, K., Kahle, H. G., & Peter, Y. (1999). 3D crustal structure from local earthquake tomography around the Gulf of Arta (Ionian region, NW Greece). *Tectonophysics*, 304, 201-218.

- Havskov, J., & L. Ottemöller (2003). SEISAN: The earthquake analysis softwares for Windows, Solaris and Linux, Version 9.0. *Institute of Solid Earth Physics*, University of Bergen, Norway.
- Hazarika, P., Kumar, M. R., Srijayanthi, G., Raju, P. S., Rao, N. P., & Srinagesh, D. (2010). Transverse tectonics in the Sikkim Himalaya: evidence from seismicity and focal-mechanism data. *Bulletin of Seismological Society of America*, 100(4), 1816-1822.
- Hazarika, D., Wadhawan, M., Paul, A., Kumar, N., & Borah, K. (2017). Geometry of the Main Himalayan Thrust and Moho beneath Satluj valley, northwest Himalaya: Constraints from receiver function analysis. *Journal of Geophysical Research: Solid Earth*, 122, 2929–2945. <https://doi.org/10.1002/2016JB013783>.
- Hetényi, G., Cattin, R., Berthet, T., Le Moigne, N., Chopel, J., Lechmann, S., Hammer, P., Drukpa, D., Sapkota, S.N., Gautier, S. & Thinley, K. (2016a). Segmentation of the Himalayas as revealed by arc-parallel gravity anomalies. *Scientific reports*, 6(1), 1-10.
- Hetényi, G., Le Roux-Mallouf, R., Berthet, T., Cattin, R., Cauzzi, C., Phuntsho, K. & Grolimund, R. (2016b). Joint approach combining damage and paleoseismology observations constrains the 1714 A.D. Bhutan earthquake at magnitude 8 ± 0.5 . *Geophysical Research Letters*, 43, 10,695–10,702. <http://dx.doi.org/10.1002/2016GL071033>.
- Holt, W. E., Ni, J. F., Wallace, T. C., & Haines, A. J. (1991). The active tectonics of the eastern Himalayan syntaxis and surrounding regions. *Journal of Geophysical Research: Solid Earth*, 96(B9), 14595-14632.
- Husen, S., Smith, R. B., & Waite, G. P. (2004). Evidence for gas and magmatic sources beneath the Yellowstone volcanic field from seismic tomographic imaging. *Journal of Volcanology and Geothermal Research*, 131, 397-410.
- Jade S., Shrungheshwara T.S., Kumar K., Choudhury P., Dumka R.K. & Bhu H. (2017). India plate angular velocity and contemporary deformation rates from continuous GPS measurements from 1996 to 2015. *Nature Scientific Reports*, 7, 11439, <https://doi.org/10.1038/s41598-017-11697-w>.
- Kayal, J. R., De, R., & Chakraborty, P. (1993). Microearthquakes at the main boundary thrust in Eastern Himalaya and the present-day tectonic model. *Tectonophysics*, 218, 375–381.
- Kayal, J.R., Arefiev, S.S., Baruah, S., Hazarika, D., Gogoi, N., Kumar, A., Chowdhury, S.N., & Kalita, S. (2006). Shillong plateau earthquakes in northeast India region: complex tectonic model. *Current Science*, 91 (1), 109–114.
- Kayal, J.R., Arefiev, S.S., Baruah, S., Tatevossian, R., Gogoi, N., Sanoujam, M., Gautam, J.L., Hazarika, D. & Borah, D. (2010). The 2009 Bhutan and Assam felt earthquakes (Mw 6.3 and 5.1) at the Kopili fault in the northeast Himalaya region. *Geomatics, Natural Hazards and Risk*, 1(3), 273-281.
- Kayal, J. R., Arefiev, S. S., Baruah, S., Hazarika, D., Gogoi, N., Gautam, J. L., Baruah, S., Dorbath, C., & Tatevossian, R. (2012). Large and great earthquakes in the Shillong plateau–Assam valley area of Northeast India Region: pop-up and transverse tectonics. *Tectonophysics*, 532, 186–192. <http://dx.doi.org/10.1016/j.tecto.2012.02.007>.
- Kaypak, B. (2008). Three-dimensional VP and VP/VS structure of the upper crust in the Erzincan basin (eastern Turkey). *Journal of Geophysical Research*, 113, B07307, doi:10.1029/2006JB004905.

- Khattari, K., Wyss, M., Gaur, V. K., Saha, S. N., & Bansal, V. K. (1983). Local seismic activity in the region of the Assam Gap, northeast India. *Bull. Seismol. Soc. Am.*, 73 (2), 459-469.
- Kissling, E. (1988). Geotomography with local earthquake data. *Reviews of Geophysics*, 26(4), 659-698.
- Kissling, E. (1995). Velest User's Guide. *Internal report 26, Institute of Geophysics, ETH Zurich, Switzerland.*
- Koulakov, I. (2009). Out-of-network events can be of great importance for improving results of local earthquake tomography. *Bulletin of Seismological Society of America*, 99, 2556–2563.
- Kumar, A., Kumar, N., Mukhopadhyay, S., & Klemperer, S.L. (2021). Tomographic Image of Shear Wave Structure of NE India Based on Analysis of Rayleigh Wave Data. *Frontiers of Earth Science*, 9:680361. doi: 10.3389/feart.2021.680361
- Kumar, S. (Ed.). (2016). *Geology of the Eastern Himalaya: Structural and Metamorphic History of Northeast India.* Springer.
- Kundu, A., Hazarika, D., Hajra, S., Singh, A.K., & Ghosh, P. (2020). Crustal Thickness and Poisson's Ratio variations in the northeast India–Asia collision zone: Insight into the Tuting-Tidding Suture zone, Eastern Himalaya. *Journal of Asian Earth Sciences*, doi: <https://doi.org/10.1016/j.jseaes.2019.104099>.
- Lienert, B. R. E., & Havskov, J. (1995). A computer program for locating earthquakes both locally and globally. *Seismological Research Letters*. 66:26–36.
- Mahesh, P., Rai, S.S., Sivaram, K., Paul, A., Gupta, S., Sarma, P.R. & Gaur, V.K. (2013). One dimensional reference velocity model and precise locations of earthquake hypocenters in the Kumaon-Garhwal Himalaya. *Bulletin Seismological Society America*, 103 (1), 328-339.
- McNamara, D.E., Yeck, W.L., Barnhart, W.D., Schulte-Pelkum, V., Bergman, E., Adhikari, L.B., Dixit, A., Hough, S.E., Benz, H.M., & Earle, P.S. (2017). Source modeling of the 2015 Mw 7.8 Nepal (Gorkha) earthquake sequence: Implications for geodynamics and earthquake hazards. *Tectonophysics*, 714, 21-30
- Marechal, A., Mazzotti, S., Cattin, R., Cazes, G., Vernant, P., Drukpa, D., Thinley, K., Tarayoun, A., Le Roux-Mallouf, R., Thapa, B., Pelgay, P., Gyeltshen, J., Doerflinger, E., & Gautier, S. (2016). Evidence of interseismic coupling variations along the Bhutan Himalayan arc from new GPS data. *Geophysical Research Letters*, 43 (12), 12399–12406. <http://dx.doi.org/10.1002/2016gl071163>.
- Monsalve, G., Sheehan, A., Schulte-Pelkum, V., Rajaure, S., Pandey, M. R., & Wu, F. (2006). Seismicity and one-dimensional velocity structure of the Himalayan collision zone: Earthquakes in the crust and upper mantle. *Journal of Geophysical Research: Solid Earth*, 111(B10).
- Monsalve, G., Sheehan, A., Rowe, C., & Rajaure, S. (2008). Seismic structure of the crust and the upper mantle beneath the Himalayas: Evidence for eclogitization of lower crustal rocks in the Indian Plate. *Journal of Geophysical Research: Solid Earth*, 113(B8).
- Nábělek, J., Hetényi, G., Vergne, J., Sapkota, S., Kafle, B., Jiang, M., et al. (2009). Underplating in the Himalaya-Tibet collision zone revealed by the Hi-CLIMB experiment. *Science*, 325(5946), 1371–1374. <https://doi.org/10.1126/science.1167719>.

- Nandy, D.R.(2001). Geodynamics of Northeastern India and the Adjoining Region. *acb Publication*, Kolkata. 209.
- Ni, J., & Barazangi, M. (1984). Seismotectonics of the Himalayan collision zone: Geometry of the underthrusting Indian plate beneath the Himalaya. *Journal of Geophysical Research: Solid Earth*, 89(B2), 1147-1163.
- Okada, H., Suzuki, S., &Asano, S. (1970). Anomalous Underground Structure in the Matsushiro Earthquake Swarm Area as Derived from a Fan Shooting Technique. *Bulletin of the Earthquake Research Institute*, Tokyo University. 48, 811-833.
- Pandey, A. K., Chingtham, P., & Roy, P. N. S. (2017). Homogeneous earthquake catalogue for Northeast region of India using robust statistical approaches. *Geomatics, Natural Hazards and Risk*, 8(2), 1477-1491.
- Pandey, M. R., Tandukar, R. P., Avouac, J. P., Lave, J., & Massot, J. P. (1995). Interseismic strain accumulation on the Himalayan crustal ramp (Nepal). *Geophysical Research Letters*, 22(7), 751-754.
- Pandey, A., Jayangondaperumal, R., Hetényi, G., Priyanka, R. S., Singh, I., Srivastava, P., & Srivastava, H. B. (2021). Establishing primary surface rupture evidence and magnitude of the 1697 CE Sadiya earthquake at the Eastern Himalayan Frontal thrust, India. *Scientific reports*, 11(1), 1-14, <https://doi.org/10.1038/s41598-020-79571-w>.
- Paul, J., Bürgmann, R., Gaur, V.K., Bilham, R., Larson, K.M., Ananda, M.B., Jade, S., Mukal, M., Anupama, T.S., Satyal, G., & Kumar, D. (2001). The motion and active deformation of India. *Geophysical Research Letters*, 28(4), 647-650.
- Poddar, M. C. (1950). The Assam earthquake of 15th August 1950. *Indian Miner*, 4(4), 167-176.
- Rajendran, K., & Rajendran, C. (2011). Revisiting the earthquake sources in the Himalaya: Perspectives on past seismicity. *Tectonophysics*, 504 (1), 75 – 88. doi: 10.1016/j.tecto.2011.03.001
- Rajendran, K., Parameswaran, R. M., & Rajendran, C. P. (2017). Seismotectonic perspectives on the Himalayan arc and contiguous areas: Inferences from past and recent earthquakes. *Earth Science Reviews*, 173, 1-30.
- Rakshit, K., and Rakshit, R. (2022). Study of 28th April, 2021 Mw 6.0 Assam earthquake in a part of eastern Himalayan foreland region, northeast India. *Environmental Earth Sciences*, 81:368. <https://doi.org/10.1007/s12665-022-10496-5>.
- Rao, N. P., & Kumar, M. R. (1997). Uplift and Tectonics of the Shillong Plateau, Northeast India. *J. Phys. Earth*, 45, 167-176.
- Schulte-Pelkum, V., Monsalve, G., Sheehan, A., Pandey, M. R., Sapkota, S., Bilham, R., & Wu, F. (2005). Imaging the Indian subcontinent beneath the Himalaya. *Nature*, 435(7046), 1222-1225.
- Seeber, L., & Arbuster, J.G. (1981). Great detachment earthquakes along the Himalayan arc and long-term forecasts. In: D.W Simpson and P.G. Richards (Editors), Earthquake Prediction, An International Review, Maurice Ewing series 4., *American Geophysical Union*, Washington, DC, 259-279.

- Shukla, N., Hazarika, D., Kundu, A., & Mukhopadhyay, S. (2022). Spatial variations of crustal thickness and Poisson's ratio in the northeastern region of India based on receiver function analysis. *Geological Journal*, 57(12), 5083–5096. <https://doi.org/10.1002/gj.4469>.
- Singer, J., Kissling, E., Diehl, T., & Hetényi, G. (2017a). The underthrusting Indian crust and its role in collision dynamics of the Eastern Himalaya in Bhutan: Insights from receiver function imaging. *Journal of Geophysical Research: Solid Earth*, 122(2), 1152–1178.
- Singer, J., Obermann, A., Kissling, E., Fang, H., Hetényi, G., & Grujic, D. (2017b). Along-strike variations in the Himalayan orogenic wedge structure in Bhutan from ambient seismic noise tomography. *Geochemistry, Geophysics, Geosystems*, 18 (4), 1483–1498. doi: 10.1002/2016GC006742.
- Singh, A., Kumar, M. R., & Raju, P. S. (2010). Seismic structure of the under-thrusting Indian crust in Sikkim Himalaya. *Tectonics*, 29 (6). doi: 10.1029/2010TC002722
- Singh, A., Saikia, D., & Kumar, M. R. (2021). Seismic imaging of the crust beneath Arunachal Himalaya. *Journal of Geophysical Research*, doi: 10.1029/2020JB020616.
- Sokos, E., Zahradnik, J. (2008). ISOL A a Fortran code and a Matlab GUI to perform multiple-point source inversion of seismic data. *Comput. Geosci.*, 34 (8), 967–977.
- Sokos, E., Zahradník, J. (2013). Evaluating centroid-moment-tensor uncertainty in the new version of ISOLA software. *Seismol. Res. Lett.*, 84 (4), 656–665.
- Stevens, V. L., & Avouac, J. P. (2016). Millenary $M_w > 9.0$ earthquakes required by geodetic strain in the Himalaya. *Geophysical Research Letters*, 43(3), 1118–1123.
- Subedi, S., Hetényi, G., Vergne, J., Bollinger, L., Lyon-Caen, H., Farra, V., et al. (2018). Imaging the Moho and the Main Himalayan Thrust in Western Nepal with receiver functions. *Geophysical Research Letters*, 45, 13,222–13,230. <https://doi.org/10.1029/2018GL080911>.
- Thurber, C.H. (1983). Earthquake locations and three dimensional crustal velocity structure in the Coyote lake area, central California, *Journal of Geophysical Research*, 88, 8226–8236.
- Thurber, C., Roecker, S., Ellsworth, W., Chen, Y., Lutter, W. & Sessions, R. (1997). Two-dimensional seismic image of the San Andreas fault in the Northern Gabilan Range, central California: evidence for fluids in the fault zone. *Geophysical Research Letters*, 24, 1591–1594.
- Geophysical Journal International*, 151, 848 – 866, doi:10.1046/j.1365-246X.2002.01812.x
- Vernant, P., Bilham, R., Szeliga, W., Drupka, D., Kalita, S., Bhattacharyya, A.K., Gaur, V.K., Pelgay, P., Cattin, R., & Berthet, T. (2014). Clockwise rotation of the Brahmaputra Valley relative to India: tectonic convergence in the eastern Himalaya, Naga Hills, and Shillong Plateau. *Journal of Geophysical Research, Solid Earth* 119 (8), 6558–6571. <http://dx.doi.org/10.1002/2014JB011196>. U.S. Geological Survey, Earthquake Hazards Program, (2017). Advanced National Seismic System (ANSS) Comprehensive Catalog of Earthquake Events and Products: Various, <https://doi.org/10.5066/F7MS3QZH>.
- Waldhauser, F., & Ellsworth, W.L. (2000). A double-difference earthquake location algorithm: Method and application to the northern Hayward fault. *Bulltein of the Seismological Society of America*, 90, 1353–1368.

- Wang, Q., Ji, S., and Xu, Z. (2009). Vp/Vs anisotropy and implications for crustal composition identification and earthquake prediction. *Acta Geol. Sin.*, 83(4), 801–815, doi:10.1111/j.1755-6724.2009.00103.x.
- Webb, A. A. G., Yin, A., & Dubey, C. S. (2013). U-Pb zircon geochronology of major lithologic units in the eastern Himalaya: Implications for the origin and assembly of Himalayan rocks. *GSA Bulletin*, 125 (3-4), 499-522. doi: 10.1130/B30626.1
- Wessel, P., & Smith, W. H. F. (1998). New improved version of generic mapping tools released. *Eos Transactions American Geophysical Union*, 79(47), 579.
- Yadav, D. K., Hazarika, D., Kumar, N., & Singh, A. K. (2021). Microseismicity study in the Siang Valley of Arunachal Himalaya: Tectonic Implication of the 2019 Mw 5.9 Mechuka Earthquake. *Himalayan Geology*, 42, 290–298.
- Yin, A., Dubey, C., Kelty, T., Webb, A., Harrison, T., Chou, C., & Clrier, J. (2010). Geologic correlation of the Himalayan orogen and Indian craton: Part 2. Structural geology, geochronology, and tectonic evolution of the Eastern Himalaya. *GSA Bulletin*, 122 (3-4), 360-395. doi: 10.1130/B26461.1.
- Zandt, G., & Ammon, C. J. (1995). Continental crust composition constrained by measurements of crustal Poisson's ratio. *Nature*, 374, 152-154. <https://doi.org/10.1038/374152a0>
- Zhao, D., Hasegawa, A., & Horiuchi, S. (1992). Tomographic imaging of P and S wave velocity structure beneath northeastern Japan, *Journal of Geophysical Research*, 97, 19909-19928, doi:10.1029/92JB00603.